universität wien

MASTERARBEIT | MASTER'S THESIS

Titel | Title

Transitions in surface mineralogy of rocky exoplanets based on atmospheric types

verfasst von | submitted by

Leon Sereinig BSc

angestrebter akademischer Grad | in partial fulfilment of the requirements for the degree of

Master of Science (MSc)

Wien | Vienna, 2025

Studienkennzahl lt. Studienblatt | Degree programme code as it appears on the student record sheet:	UA 066 861
Studienrichtung lt. Studienblatt | Degree programme as it appears on the student record sheet:	Masterstudium Astronomy
Betreut von | Supervisor:	Oliver Herbort B.Sc. M.Sc. PhD

Abstract

The surfaces of terrestrial exoplanets are currently unobservable because of the small sizes of the planets and the vast distances from our solar system. If an atmosphere is present, such observations become even more difficult, since the atmosphere obscures the surface. However, transit observations, where the exoplanet crosses its host star from our point of view, allow for measurements of an atmospheric spectrum and therefore determine the atmospheric composition. If the link between atmospheric and surface composition is understood, such transit observations could make the surface composition indirectly observable.

This thesis investigates the nature of the link between atmospheres and crusts of terrestrial exoplanets at temperatures from 500 K to 1000 K. Atmospheres are classified by type, which necessitates the expansion of the established atmospheric type system to temperatures beyond 600 K.

Thermo-chemical and phase equilibrium models of atmosphere-crust pairs were calculated. These models were inspired by rock compositions found on earth and bodies of the solar system, including asteroid sample return missions. To accurately model the universes possible diversity, multiple grids across a atmospheric parameter space, based on the elements carbon, hydrogen, and oxygen (CHO), were generated. The atmosphere-crust link was examined at six temperatures, ranging from 500 K to 1000 K in 100 K increments.

Several crust compounds exhibited links to the atmospheres type, most notably sulphur containing compounds with a sequence of crust condensates existing contacting atmospheres from reducing to oxidising compositions: FeS[s], FeS_2[s], and $CaSO_4$[s]. Similarly iron containing compounds form a sequence in redox potential throughout the CHO atmospheric parameter space. Sharp transitions in crust compounds are visible at atmospheric type borders in the CHO atmospheric parameter space. These results bring the characterisation of crust compositions from atmospheric observations a step closer to reality.

Kurzfassung

In dieser Arbeit wurde die Interaktion zwischen Atmosphären und Oberflächen von Gesteins-Exoplaneten untersucht. Wegen der enormen Distanzen zu Exoplaneten sind diese mit heutiger Technologie nicht direkt auflösbar. Wenn eine Atmosphäre vorhanden ist dann kann diese unter Umständen die Oberfläche verdecken, was Beobachtungen der Oberflächenkomposition unmöglich macht. Über Transitbeobachtungen können jedoch Spektren gemessen werden, welche Rückschlüsse auf die atmosphäische Zusammensetzung erlauben. Wenn der Zusammenhang zwischen atmospärischer- und Oberflächenkomposition bekannt ist kann die Oberfläche indirekt beobachtet werden.

Diese Arbeit untersucht den Zusammenhang zwischen atmosphärischer- und Oberflächenkomposition bei Temperaturen von 500 K bis hin zu 1000 K. Atmospähren wurden nach Typen klassifiziert, was die Ausweitung des etablierten Atmosphären-Typen Systems zu Temperaturen über 600 K verlangt.

Dafür wurden Modelle im thermo-chemischen und Phasengleichgewicht von Atmosphären-Oberflächen Paaren berechnet. Diese Modelle sind inspiriert von erdähnlichen Kompositionen und von Gesteinen des Sonnensystems, unter anderem auch von zurückgeholten Asteroidenproben. Um die Vielfalt des Universums in den Modellen wiederzuspiegeln wurde ein atmosphärischer parameterbereich basierend auf den Elementen Kohlenstoff, Wasserstoff und Sauerstoff (CHO) systematisch mit Atmosphären-Oberflächen Modell-paaren abgedeckt. Die Atmosphären und Oberflächen Interaktion wurde bei sechs Temperaturen untersucht, von 500 K bis 1000 K in 100 K Schritten.

Eine Reihe an Oberflächenkondensate weisen eine klare Verbindung zum Typen der zugehörigen Atmospähre auf, darunter schwefel- und eisenhaltige Kondensate. Beide Kondensatgruppen bilden eine Sequenz in Redoxpotential, mit den schwefelhaltingen Kondensaten FeS[s], FeS_2[s] und $CaSO_4$[s]. Scharfe Übergänge der Oberflächenkomposition sind ident zu Atmosphärentypengrenzen im CHO Parameterbereich.

Contents

1 Introduction

Since the discovery of the first exoplanets orbiting a pulsar (Wolszczan & Frail 1992) in the year 1992, followed by the detection of 51 Pegasi orbiting a main sequence star (Mayor & Queloz 1995), the number of exoplanet detections has grown to over 7000[1]. About 12% of these may be terrestrial worlds [2]. This may be an under-representation of the actual terrestrial exoplanet population. This is because of lower mass and lower size compared to gas giants, detection is more difficult, therefore it is likely that terrestrial exoplanets are more abundant as detections currently suggest. Thanks to multiple detection methods for exoplanets, such as the transit method or the radial velocity method, a range of parameters can be obtained, for example, the planets size, mass, density, and temperature (e.g. Mayor & Queloz 1995; Henry et al. 2000; Charbonneau et al. 2000). The transit method does not only provide a constraint on the size of a given planet, it also offers the unique opportunity to study the atmosphere of exoplanets (Charbonneau et al. 2002). This is because the light originating from the star passes through the planets atmospheres where atmospheric particles absorb the stars light. Since the atmospheres molecules absorb light at very specific wavelengths it is then possible to measure compositions of exoplanets atmospheres by measuring transit spectra (e.g. Richardson et al. 2007; Pont et al. 2008). This kinds of observations are difficult to obtain since planets are usually only a fraction the size of their host stars and therefore their atmospheres are even smaller than that, meaning that most of the host stars light remains unobstructed during a transit. Additionally, scattering can make the transmission of light through the planets atmosphere even lower. Consequentially, smaller host stars and bigger planets yield higher signal to noise ratios with current instrumentation, allowing for more detailed study than planets orbiting sun-like stars or even larger stars (e.g. Wakeford et al. 2013; Wyttenbach et al. 2015; Rustamkulov et al. 2023).

Due to the small size of terrestrial planets, characterising them is even more difficult. It has been possible to derive parameters such as size and mass (e.g. Léger et al. 2009; Batalha et al. 2011) of such rocky planets for over a decade. Detections of rocky exoplanet atmospheres are currently being attempted and often point to airless worlds (e.g. Xue et al. 2025; Ducrot et al. 2025; Piaulet-Ghorayeb et al. 2025). This can either be caused by thin atmospheres which are below current instruments detection limits, or can be attributed to detection bias. Since planets which orbit small stars (e.g. M-dwarves) naturally produce deeper transit curves which are easier to detect. Current research suggests that planets orbiting M-dwarf stars, are subjected to strong XUV-emissions and are stripped of any atmosphere early on (Van Looveren et al. 2025), leading to many non-detections of atmospheres of planets orbiting M-dwarves. With current and future space based observatories like the James Webb Space Telescope (JWST) (Gardner et al. 2023), the Ariel space mission (Tinetti et al. 2018), the PLAnetary Transits and Oscillation of stars

[1] `https://exoplanet.eu/home/` accessed April 2025

[2] Based on exoplanet.eu fraction of detected planets with $R_p < 1.5 R_{earth}$

(PLATO) mission (Rauer et al. 2025), the CHaracterising ExOPlanet Satellite (CHEOPS) (Benz et al. 2021), or ground based telescopes of the next generation such as the Extremely Large Telescope (ELT) (Gilmozzi & Spyromilio 2007), it is already possible to detect atmospheres of large (1.95 R_{Earth},8.8 M_{Earth}) rocky worlds (Hu et al. 2024), and detections will likely become more frequent in the future. Future observational capabilities will also allow observations of earth sized exoplanets.

When characterising terrestrial exoplanets, a further important parameter is the surface composition. Using methods like polarimetry, reflection or emission spectroscopy, a handful of solar system body properties have been measured (e.g. Madden & Kaltenegger 2018), which could be used for reference for exoplanets. In the case of exoplanets, because of their small diameters and vast distances, it is difficult to directly observe the surface. If a terrestrial exoplanet possesses an atmosphere these methods become more difficult. Similarly like infrared astronomy has to constrain itself to atmospheric windows, or like ground based UV astronomy being possible since the earths atmosphere is obscuring these wavelengths, it will be just as difficult for an observer trying to study earths surface looking in from the outside. An extreme example would be if one were to try measure the Venusian surface composition, where the dense atmosphere and a planet wide cloud layer only allow for very slim windows of transparency (multiple narrow bands around 1.02 µm, 1.1 µm, 1.18 µm, 1.27 µm, and 1.31 µm: Helbert et al. (2008), Kappel et al. (2016), Gilmore et al. (2017)). This means that in some cases the direct observation of a terrestrial exoplanets crust will be virtually impossible. Thanks to Venus' proximity to Earth it can be used as a blueprint to inspire the modelling of such planets. In the seventies and eighties the Venera and Vega landers were deployed to the Venusian surface, and were able to measure rock compositions (see Surkov et al. 1983, 1986). The results of these landers can inform modelling of Venusian conditions (e.g. Rimmer et al. 2021) which can also be applied towards exoplanet modelling (e.g. Jordan et al. 2021).

The existence of clouds and hazes can further obscure the surface via scattering. In some cases making measuring the atmospheric composition impossible, by instead of absorbing specific wavelengths of light, absorbing all light (Berta et al. 2012) making the atmosphere fully opaque. In less extreme cases, where only the crust is obscured, modelling the chemistry for atmospheres and surfaces could provide an insight in the otherwise unobservable surface parameters. An atmosphere in contact with the surface can be described by a chemical system in exchange either due to kinetic chemistry or by weathering processes, driven by rain, where rock can dissolve in the droplets, and fluids and gas exert mechanical friction. Systems without such weathering processes can only equilibrate with processes such as annealing where solid material is hot enough to allow for rearrangement. Understanding the link between the atmosphere and crust is instrumental in characterising exoplanet surface mineralogical compositions, and would allow to infer the crusts composition by observing only the atmospheres composition. Past works have already been able to show that certain surfaces properties can be connected to atmospheric compositions (including cloud compositions), like the outgassing of rock (Schaefer et al. 2012), the existence of liquid water (Herbort et al. 2020), surface pressure linked to cloud condensates (Herbort et al. 2022), surface composition linked to a pressure-temperature profile (Byrne et al. 2024), and the connection between atmospheric composition and surface composition (Herbort & Sereinig 2025).

Research on atmosphere formation suggests that secondary atmospheres form from outgassing (e.g. Schaefer et al. 2012; Wordsworth & Kreidberg 2022; Gaillard & Scaillet 2014). These atmospheres form early on, when the planets are still hot, potentially molten, and therefore the surface and atmosphere can reach thermo-chemical equilibrium relatively quickly (Lichtenberg & Miguel 2025). However, as planets become cooler over time, the time it takes to reach equilibrium grows. For planets with constant volcanic activity and a temperature of $T < 700\,\mathrm{K}$ it has been suggested that equilibrium may never be reached due to long chemical timescales (Liggins et al. 2023).

For physical modelling of exoplanet atmosphere-crust pairs, inspiration can be drawn from solar system objects. Since there are only a handful terrestrial bodies with substantial atmospheres in our solar system, namely Venus, Earth, and Titan, these can not reflect the potential diversity of all possible planet-atmosphere compositions in the universe. This thesis aims to reflect that diversity by building on geological research as a starting point for the modelling of crust-atmosphere pairs. It employs elemental compositions such as MORB (Arevalo & McDonough 2010), (exo)planetary science, with the elemental compositions of Earth (Herbort et al. 2022), BSE and CC (Schaefer et al. 2012), and compositions of material from the solar system, such as CI-Chondrite (Lodders et al. 2009) and material retrieved from the asteroid Ryugu (Yokoyama et al. 2025). The abundances of volatiles hydrogen, oxygen, and carbon are systematically varied, while the remaining mostly refractory elements are kept constant. To generate crust-atmosphere models, this thesis employs a bottom-to-top equilibrium chemistry model, for calculating crust mineral composition and atmospheric composition. One advantage of using an equilibrium chemistry approach, is that it enables a diverse set of input elements (which are needed for crust mineral formation), since the complete chemical kinetic network does not exist for some species, and is often limited to the elements carbon, hydrogen, nitrogen, and oxygen (CHNO) (e.g. Yang & Hu 2024). Additionally, the computation time is short compared to models that take disequilibrium processes into account, which enables the investigation of a large range of diverse models.

The goal of this thesis is to investigate the link between exoplanet atmospheres and their corresponding crustal compositions. This link is connected with a wide range of parameters, such as atmospheric surface pressure, surface temperature, atmospheric gas composition, and availability of different element species. This work will focus on the latter three parameters, as the atmospheric gas pressure will be kept at a constant 1 bar. In Sect. 2, the general methodology will be laid out, including a description of the chemical modelling. The choice of equilibrium chemistry is discussed in Sect. 2.2, and the systematic probing of diverse atmospheric compositions in Sect. 2.3. In Section 3 the results are shown, including an expansion of the atmospheric type classification system in Sec 3.1.1. This is followed by a description of the link between crust condensates and atmospheric composition in Sect. 3.2, with a more detailed description of sulphur compounds in Sect. 3.2.1 and iron oxidation state in the crust Sect. 3.2.2. Further, manganese containing, condensates link to the atmosphere is shown in Sect. 3.2.3, and remaining minor condensates links to the atmosphere in Sect. 3.2.4. The limits and implications of the results are discussed in Sect. 4. A summary is provided in Sect. 5.

2 Methodology

This thesis employed thermo-chemical and phase equilibrium modelling to generate crust-atmosphere pairs using the equilibrium chemistry solver GGchem (Woitke et al. 2018). Surface temperature and availability of element species are input parameters and therefore easy to control and probe. The atmospheric gas composition is an output parameter and does not have a linear relation between input elements and output composition. This calls for a robust and systematic approach, in order to generate a diverse enough sample of atmospheric compositions. To achieve this, an atmospheric parameter space based on the most abundant atmospheric elemental species carbon C, hydrogen H, nitrogen N, and oxygen O, (the CHNO system) from (Woitke et al. 2021; Herbort et al. 2020, 2022) which also introduces atmospheric types was used. The link of certain crust condensates to atmospheric type was first probed in Herbort & Sereinig (2025).

2.1 Chemical modelling

For the modelling of crust-atmosphere pairs, the thermo-chemical equilibrium was solved with GGchem (see Woitke et al. 2018). GGchem allows the input of any elemental abundance, temperature, and pressure. It then computes the composition of the system using the principle of minimising Gibbs free energy of formation $\Delta G_{\rm f}^{\ominus}$ of a molecule or particle at a standard pressure $p^{\ominus}$. For an arbitrary molecule $\mathrm{A}_a\mathrm{B}_b\mathrm{C}_c$ it can be calculated using

$$\Delta G_{\rm f}^{\ominus} = G^{\ominus}(\mathrm{A}_a\mathrm{B}_b\mathrm{C}_c, T) - aG^{\ominus}(\mathrm{A}, T) - bG^{\ominus}(\mathrm{B}, T) - cG^{\ominus}(\mathrm{C}, T), \tag{2.1}$$

where A, B, and C are the elements making up the molecule, a, b, and c are their respective stoichiometric factors, and T denotes the temperature of the system. $G^{\ominus}$ is the Gibbs free energy at a reference pressure $p^{\ominus}$ which is defined as

$$G^{\ominus}(\mathrm{A}, T) = H(\mathrm{A}, T) - T \cdot S(\mathrm{A}, T), \tag{2.2}$$

where $H(\mathrm{A}, T)$ is the enthalpy of the element A at the temperature T and $S(\mathrm{A}, T)$ is the entropy of the element A at the temperature T. Utilising Guldbergs law of mass action it is then possible to express molecular partial pressures as

$$p_{\mathrm{A}_a\mathrm{B}_b\mathrm{C}_c} = k_p(\mathrm{A}_a\mathrm{B}_b\mathrm{C}_c, T) \cdot p_{\mathrm{A}}^a p_{\mathrm{B}}^b p_{\mathrm{C}}^c, \tag{2.3}$$

where p_x is the partial pressure of the molecule or elemental species, and k_p are the equilibrium constants at a given reference pressure p for transferring elemental partial pressures to molecular partial pressures, which are given as

$$k_p(\mathrm{A}_a\mathrm{B}_b\mathrm{C}_c, T) = (p^{\ominus})^{1-a-b-c} \cdot \exp(-\Delta G_{\rm f}^{\ominus}/RT). \tag{2.4}$$

Here R denotes the ideal gas constant. By finding the minimal energy of formation of a molecular gas composition, and expressing the partial pressures of each molecular species as the elemental pressures, and using the ideal gas law $p = nkT$ it is then possible to solve for partial pressures of each molecular species with

$$\epsilon_k n_{(\mathrm{H})} = \sum_i s_{i,k} n_i, \tag{2.5}$$

with ϵ_k being the elemental abundance for the element k normalized to hydrogen abundance, $n_{(\mathrm{H})}$ is the hydrogen abundance, $s_{i,k}$ is the stoichiometric factor of the element k in the molecule i, and n_i are the molecular particle densities. Equilibrium condensation is used to include the crust formation in the modelling approach. Equilibrium condensation works by expressing vapour pressure $p_j^{\mathrm{vap}}(T)$ (the partial pressure of condensate species j when it is in phase equilibrium with the condensed phase of itself) as

$$p_j^{\mathrm{vap}}(T) = p^{\ominus} \exp\left(\frac{G^{\ominus}(j(\mathrm{cond}), T) - G^{\ominus}(j, T)}{RT}\right), \tag{2.6}$$

and then defining the supersaturation ratio S_j as

$$S_j = \frac{p_j}{p_j^{\mathrm{vap}}(T)}, \tag{2.7}$$

with p_j the species partial pressure in the gas phase. If this ratio is below 1, no condensate of this species is thermally stable and therefore not present. When the ratio is above 1 condensates are stable and the ϵ_k of the gas phase are reduced until $S_j = 1$ is reached. In phase equilibrium it is not possible to reach values of $S_j > 1$. By transforming Eq. 2.7 using Equations 2.3 and 2.4, it is possible to express the supersaturation ratio of condensates without the usage of a gaseous pressure p_j as

$$S_{A_a B_b C_c} = \left(\frac{p_A}{p^{\ominus}}\right)^a \left(\frac{p_B}{p^{\ominus}}\right)^b \left(\frac{p_C}{p^{\ominus}}\right)^c exp\left(-\frac{\Delta G_{\mathrm{f}}^{\ominus}}{RT}\right). \tag{2.8}$$

This is essential for many solid mineral species which have no stable gaseous counterpart at atmospheric conditions, which would make Eq. 2.7 not applicable.

With this, it is possible to simulate exoplanet crusts-atmosphere pairs. The gas phase of GGchem's output is interpreted as the atmosphere, and the condensed species are interpreted as the crust composition of a terrestrial exoplanet. The atmospheric input pressure was specified as a constant 1 bar and a constant surface temperature was assumed. The elemental input abundances consisted of 18 element abundances, including H, C, N, O, F, Na, Mg, Al, Si, P, S, Cl, K, Ca, Ti, Cr, Mn, and Fe. With these elements GGchem includes 471 gaseous particles in the calculation including molecules, atoms, and ions, with 223 condensed species, of which 46 are liquid. The equilibrium constants used are from Stock (2008), Barklem & Collet (2016), and Woitke et al. (2018).

In order to investigate the temperature behaviour of the crust-atmosphere link, the temperature was varied from 500 K to 1000 K in 100 K increments. Since this work focuses on the crust-atmosphere interaction and convective mixing effects were omitted, an assumption of a pressure

temperature structure was not required. Instead, the composition of a single atmospheric 'cell' at constant surface pressure and temperature was calculated. In an approximation the composition of this cell was interpreted as the composition of the whole atmosphere, also referred to as the near-crust atmosphere in Herbort et al. (2020). Atmospheric chemistry like cloud formation, or compositional changes due to temperature and pressure using a full pressure-temperature structure have been investigated in previous works (e.g. Herbort et al. 2020, 2022; Herbort & Sereinig 2025).

2.2 Assumption of equilibrium

The presence of thermo-chemical and phase equilibrium between crust and atmosphere is not a given. Various disequilibrium processes like volcanism, photochemistry and atmospheric escape induced by stellar radiation, or impact events can disrupt or prevent thermo-chemical equilibrium altogether. Volcanic gases are often drastically hotter than the atmosphere itself, which can introduce molecular species that should not exist at the atmospheres pressure and temperature according to equilibrium chemistry. An example for this is Earths atmosphere, in which according to equilibrium chemistry the species N_2, O_2, CO_2, and H_2O (see also Tab. 2.1) can coexist in equilibrium. However, presence of lifeforms cause CH_4 gases to exist, and volcanoes or a forest fire can emit carbon monoxide (CO) gases. Furthermore, equilibrium timescales rise dramatically for lower temperatures, which can lead to systems that may never reach equilibrium. Current research suggests that atmospheres with a temperature below 700 K with constant volcanism never reach chemical equilibrium (Liggins et al. 2023). However any system, whether it can reach equilibrium or not, always evolves towards equilibrium. If disequilibrium processes can be ignored in a first order approximation for disequilibrium processes at moderate levels, modelling using equilibrium chemistry should not yield drastically different results form reality. This is shown in Herbort et al. (2022), where an equilibrium chemistry atmospheric model composition of earths atmosphere is within a couple ppm of earths actual atmospheric composition, with the exception of methane CH_4. This is despite earth experiencing a multitude of disequilibrium processes such as volcanism, atmospheric escape, and harbouring an extensive ecosystem.

The investigation of disequilibrium processes lies beyond the scope of this thesis. Since the term 'disequilibrium processes' includes a large amount of various different processes, many of which are not fully understood, the inclusion of only a couple of those would not make the model complete. Stellar parameters depend on the planets host stars type and the distance between star and planet, which would introduce two new parameters to the model. If included, lighter species such as H_2 could be depleted via atmospheric escape driven by stellar winds, and photochemistry could destroy species such as CH_4, NH_3, or H_2O (Tsai et al. 2024). Additionally, due to computational constraints, models including such disequilibrium processes, have to limit the chemical networks to only include a handful of elements such as carbon, hydrogen, nitrogen, oxygen, and sulphur, also referred to as the CHNOS elements and incomplete reaction equations (e.g. Jordan et al. 2021). In contrast, equilibrium chemistry modelling enables a large number of chemical compounds to be included with relatively short computation times, and therefore allows for more diverse datasets to be generated.

2.3 Atmospheric grid

In order to reflect the real-life terrestrial exoplanet populations possible diversity, a diverse sample of exoplanet atmospheres was generated. Since the crusts composition is hard to predict, as it is an 18 dimensional problem consisting of 18 elements and 223 possible condensates, the atmospheric composition was used as a guide to replicate the diversity of real life. Even though with 18 input elements GGchem would in theory allow for 471 atmospheric species to form, the bulk of the atmospheric compounds are only made up of few elements. This holds true for the conditions examined in this work, which are 1 bar and temperatures ranging from 500 K to 1000 K in 100 K increments. These species are mainly consisting of elements from the CHNOS system. Sulphur is the least abundant element and is only found in the atmosphere under very specific conditions (see Sect. 3.2.1.2). Nitrogen, while abundant, does not strongly interact with the other four elements but rather interacts with itself, forming N_2 in many cases. Considering this, the input elements S and N do not heavily affect the final atmospheric composition. The elements C, H, and O include most of the chemical interactions in the atmospheres investigated here.

For a diverse grid of atmosphere-crust model pairs, a set of models with identical elemental input abundance but varying C,H and O abundances was generated. This grid should cover the span of an atmospheric parameter space introduced by Woitke et al. (2021). This approach isolates the effect the atmospheric composition has on the crust, since most crust-forming elements in the input are constant across the entire grid of atmospheric compositions. The atmospheric parameter space relates C, H, and O as

$$\frac{O-H}{O+H} \quad \text{and} \quad \frac{C}{H+O+C}, \tag{2.9}$$

for the y and x axis, respectively. The y axis reaches values from -1 to +1, where a pure hydrogen atmosphere would have a value of -1, and a pure oxygen atmosphere would have a value of +1. The x-axis introduces atmospheric carbon abundance, in relation to total C, H, and O abundances. The parameter space also defines atmospheric types up to 600 K based on which molecules can coexist in chemical equilibrium, listed in Table 2.1. Type A atmospheres are a reducing class of atmospheres with the atmospheric species H_2O, CH_4, NH_3, H_2 or N_2 coexisting. H_2 and NH_3 are exclusive to this type. Type B is an oxidising atmospheric type with the species H_2O, CO_2, O_2, and N_2 in coexistence. Molecular oxygen (O_2) is unique to atmospheres of type B. Type C atmospheres contain a blend of type A and B atmospheric types species, with H_2O, CO_2, CH_4, and N_2, and no unique species. Type D atmospheres contain CO_2, CH_4, CO, and N_2, with CO being unique to this type. The atmospheric parameter space is also shown in Fig. 2.1, including positions of atmospheres of terrestrial solar system bodies.

The original parameter space following Woitke et al. (2021) does not include sulphur. However, if sulphur quantities are sufficient, atmospheric subtypes with distinctive chemical properties can arise. The parameter space has previously been expanded by the inclusion of sulphur by Janssen et al. (2023). There, 10 atmospheric (sub)types including the sulphur species H_2S, SO_2, S_8, H_2SO_4, and SO_3 have been characterised. Since this work employs the parameter space based on just C, H, and O abundances, if an atmospheric model falls in such a subtype, it will appear to be the same as an atmosphere not in a subtype with similar C, H, and O ratios. However the

Type A:	H_2O, CH_4, NH_3, H_2 or N_2
Type B:	H_2O, CO_2, O_2, N_2
Type C:	H_2O, CO_2, CH_4, N_2
Type D:	CO_2, CH_4, CO, N_2

Table 2.1: Atmospheric types and molecular species coexisting in thermo-chemical equilibrium.

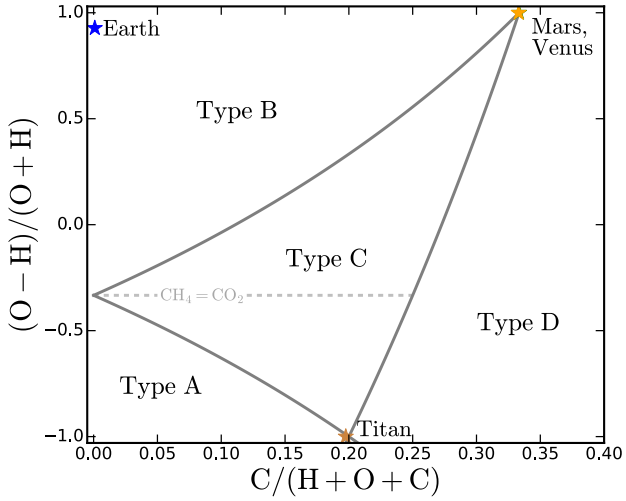

Figure 2.1: Atmospheric parameter space and atmospheric types based on Woitke et al. (2021). Substantial atmospheres of terrestrial solar bodies indicated for reference. Gray solid lines indicate atmospheric type borders (see 2.1). The dashed gray line shows where methane and carbon dioxide abundances are equal. From Herbort & Sereinig (2025).

model can have different chemical properties in the crust and atmosphere. This is discussed in Sect. 3.2.1.2.

2.3.1 Elemental inputs

Using this framework, a script was developed during this thesis which automatically creates an atmospheric parameter space-spanning grid of crust-atmosphere pairs using BASH, PYTHON, and the FORTRAN code GGCHEM. The input is a list of 18 elements, a constant pressure of 1 bar, and a constant surface temperature. The C, H, and O abundances of each crust-atmosphere pair vary slightly, but the sum of their abundances is set as constant. This ensures that the remaining 15 input elements abundances are constant in every grid point. The input elements are based on planetary research, geological science, and sample return missions. One is an Earth inspired input abundance (Earth), taken from Herbort et al. (2022), which under Earth like conditions (1.013 bar, 288.15 K) reproduces Earths atmospheric composition with equilibrium chemistry. Also inspired by Earth are Continental Crust (CC), Bulk Silicate Earth (BSE)(both Schaefer et al. 2012), and Mid Oceanic Ridge Basalt (MORB) (Arevalo & McDonough 2010). Inspired

by the very rocks that form planets, asteroids, are CI Chondrite (CI) (Lodders et al. 2009), and the composition of the asteroid Ryugu Yokoyama et al. (2025). Ryugus elemental abundances were measured by analysing material collected by the sample return mission Hayabusa-2. Since measures of fluorine (F) abundance were not done on the returned samples, it was substituted by taking the value from CI and multiplying it by a factor f defined as

$$f = \frac{1}{17} \sum_{i=1}^{17} \frac{\epsilon_{\mathrm{Ryugu},i}}{\epsilon_{\mathrm{CI},i}}, \tag{2.10}$$

where the $\epsilon_{\mathrm{abundance},i}$ are element abundances of Ryugu and CI, respectively. Since fluorine could not be included only the remaining 17 elements were used for this factor f. A complete list of the used input abundances are given in Table 2.2. One grid per elemental input abundance and per temperature was calculated. This was done in order to eliminate biases, introduced by the individual elemental input abundances. This way, if a certain crust compound appears to be linked to the atmospheric composition in one grid but not the other, it can be ruled out as a compound which formed because of the elemental ratios that were specified in the input abundance and not the atmospheric composition. A crust compound can only be considered linked to the atmospheric composition if it is present in all grids.

2.3.2 Grid generation

A BASH script was developed to automatically run GGCHEM using a specified input composition. It utilises a set of grid coordinates which are to be reached by the resulting atmospheric composition from a GGCHEM run. The script works iteratively by first running the input composition through GGCHEM as is, reading the C, H, and O abundances of the resulting atmosphere, and calculating the position of the generated atmosphere in the atmospheric parameter space. The script establishes the nearest grid coordinate and adjusts the input C, H, and O abundances accordingly in order to reach this coordinate within the next generated 2-3 atmospheric compositions. Since the remaining 15 other input elements should remain constant, each adjustment of C, H and O abundance has to fulfil the condition

$$C + H + O = const. \tag{2.11}$$

Because of this constraint it was not possible to generate oxygen dominated type B atmospheric models using the elemental inputs MORB and BSE. This is because the sum of the abundances is so small that even if the entire budget is used for oxygen abundance the resulting atmosphere will be nitrogen (N_2) dominated, to the point where the type B characteristic species are only present in trace amounts, making the type classification pointless.

To move along the x axis of the parameter space only the C abundance needs adjustment whereas movement along the y axis requires the O and H to be changed simultaneously. When moving along the x-axis the condition from Eq. 2.11 has to be fulfilled, therefore H and O also have to change simultaneously. To avoid movement along the y axis the condition

Table 2.2: Elemental mass fractions of the sets of element abundances used in this work.

	Earth	CC	CI	Ryugu	MORB	BSE
	1	2	3	4	5	2
H	0.3341	0.045	1.992	1.034159	0.023	0.006
C	1.957	0.199	3.520	4.514885	0.019	0.006
O	50.1	47.2	46.420	39.694165	44.5	44.42
N	0.0253	0.006	0.289	0.146115	5.5E-05	8.8E-05
F	0.0482	0.053	0.0059	0.0241 ∗	0.017	0.002
Na	2.145	2.36	0.505	0.612898	2.012	0.29
Mg	1.999	2.20	9.790	11.126626	4.735	22.01
Al	7.234	7.96	0.8680	0.917588	8.199	2.12
Si	26.17	28.8	10.820	12.613700	23.62	21.61
P	0.0691	0.076	0.098	0.130840	0.057	0.008
S	0.0636	0.07	5.411	5.729325	0.11	0.027
Cl	0.0427	0.047	0.071	0.077981	0.014	0.004
K	1.945	2.14	0.055	0.052457	0.152	0.02
Ca	3.499	3.85	0.933	1.397637	8.239	2.46
Ti	0.3644	0.401	0.046	0.047633	0.851	0.12
Cr	0.0118	0.013	0.268	0.269418	0.033	0.29
Mn	0.0654	0.072	0.195	0.250123	0.132	0.11
Fe	3.926	4.32	18.710	20.067360	7.278	6.27

∗: Value substituted as described in Eq. 2.10.
1: Herbort et al. (2022) 2: Schaefer et al. (2012) 3: Lodders et al. (2009) 4: Yokoyama et al. (2025) 5: Arevalo & McDonough (2010)

$$\frac{O}{H} = const \tag{2.12}$$

is introduced. The abundances are adjusted by the BASH script following a scheme like

$$\begin{aligned} C' &= C \cdot (1 \pm \alpha), \\ H' &= H \cdot (1 \pm \beta_H), \\ O' &= O \cdot (1 \mp \beta_O), \end{aligned} \tag{2.13}$$

where C', H', and O' are the newly adjusted abundances and C, H, and O the initial abundances. α and β are values that adjust the initial abundances, with α being determined by measures informed by the x-axis and β by the y-axis of the atmospheric parameter space.

High oxygen and hydrogen abundances are opposite on the y-axis, so both are adjusted inversely to each other. Since hydrogen abundances are usually drastically lower than oxygen abundances,

β_H is lower by a factor of 10 compared to β_O. The magnitudes of α and β depend on the distance between the current atmospheres position in the parameter space to the grid coordinate which is currently approached. For this α and β contain two separate 'distance functions' one for each axis. On the x-axis, which is tied to carbon abundance, values vary heavily across the span of the parameter space, with the left side approaching near 0. This influences the possible step size since C' is directly tied to the initial C abundance. To stabilise the step size on the x-axis α additionally contains an 'abundance function', which boosts the value of alpha when C abundances are low. In contrast β_H and β_O only contain the 'distance function', because by adjusting both species abundances at the same time, step size does not vary as much, and an 'abundance function' is not needed.

If the current atmospheric compositions position in the atmospheric parameter space is far from the grid coordinate which is currently approached, large changes in C, H, and O are required to keep the number of iterations and computing time low. Large changes in oxygen and hydrogen abundances can cause the sum criterion in Eq. 2.11 to produce negative C abundances. If that would be the case then an if statement takes over and rescales the new O + H sum to the old O + H sum, while keeping the newly set O/H ratio. Since hydrogen abundance is often very low compared to oxygen abundance, if large changes in abundance are required due to far distances in the parameter space to cover, hydrogen abundance can become negative. In this case another if statement sets the new H abundance to an arbitrarily low value of 10% of the original hydrogen abundance, which usually delivers the desired effect of a very low hydrogen abundance.

Ideally, any grid coordinate is reached by performing 2-3 iterations. The script declares 'success' when the resulting atmospheres coordinates absolute distance from the grid coordinate in the atmospheric parameter space is less than a specified distance. If that condition is fulfilled the grid coordinate is deleted and the code moves on to the next one. In the script there are two failure modes where the coordinate is deleted even though no atmospheric composition came near enough to trigger the 'success' criterion: if after 20 iterations the grid coordinate is not reached by an atmospheric composition, or if the absolute distance of three subsequent calculated atmospheric composition to the grid coordinate does not change by ≤ 0.001. Since each calculated atmosphere is a fully fledged data point with crust-atmosphere compositions, even if its position does not match with a grid coordinate position, it is saved and becomes a part of the final grid. This makes the final grid more finely sampled, but also less regular compared to a grid made up of only data points fulfilling the 'success' criteria. It takes around 24-48 hours to generate a full grid of atmospheres to span the atmospheric parameter space. One grid contains several thousand models based on one input set of total element abundances.

3 Results

The results section is twofold. First in Sect. 3.1 the temperature evolution of atmospheric types beyond 600 K is explored. The second part, Sect. 3.2, describes the atmosphere-crust link by grouping different condensate species into subgroups. In Sect. 3.2.1, the link between sulphur containing condensates and the atmosphere is laid out. In Sect. 3.2.2 the connection of the iron oxidation state of the crust and iron containing species to the atmosphere is described. Section 3.2.3 explores the connection of two manganese containing condensate species to the atmospheres composition, and Sect. 3.2.4 describes the link between further minor condensate species and the atmospheric composition.

3.1 Atmospheric types

The atmospheric type system described in Sect. 2.3 introduced by Woitke et al. (2021) has been established for temperatures up to 600 K. Since this thesis investigates the crust-atmosphere link for temperatures from 500 K to 1000 K, the validity of the type classification for these higher temperatures has to be investigated, which is done in Sect. 3.1.1.

Because the atmospheric types defined by Woitke et al. (2021) are based on the four-element CHNO system, but models used in this work also include sulphur, sulphur-rich atmospheric subtypes can potentially exist. These atmospheric subtypes have been characterised by Janssen et al. (2023) for temperatures up to 600 K. The influence of atmospheric sulphur is discussed in Sect. 3.1.2.

3.1.1 Temperature evolution of atmospheric types

The definition of an atmospheric type is based on which atmospheric molecular species can co-exist in thermo-chemical equilibrium with abundances above trace abundances ($n_\mathrm{i}/n_\mathrm{tot} \geq 10^{-9}$). The gas phase molecular species which define these types are O_2, H_2, NH_3, CO_2, CH_4, H_2O and CO. Other abundant molecular species such as N_2 can be found across all types. For temperatures below 600 K, type A and C atmospheres differentiate themselves, with type A atmospheres containing large H_2 and NH_3 abundances, while type C atmospheres only contain these species in trace abundances. Type C atmospheres contain CO_2, which is only found in trace abundances in type A atmospheres if the elemental compositions are close to the transition to type C atmospheres. Both atmospheric types contain CH_4.

For temperatures beyond 600 K a significant rise in H_2 abundances can be observed in type C atmospheres (in excess of trace abundance $> 10^{-3}\, n_\mathrm{i}/n_\mathrm{tot}$). Simultaneously in type A atmospheres, NH_3 abundances drastically drop and CO_2 abundances rise. In both types a rise of CO abundance can be seen as temperatures increase. As shown in Fig. 3.1, by 600 K H_2 is in excess of trace

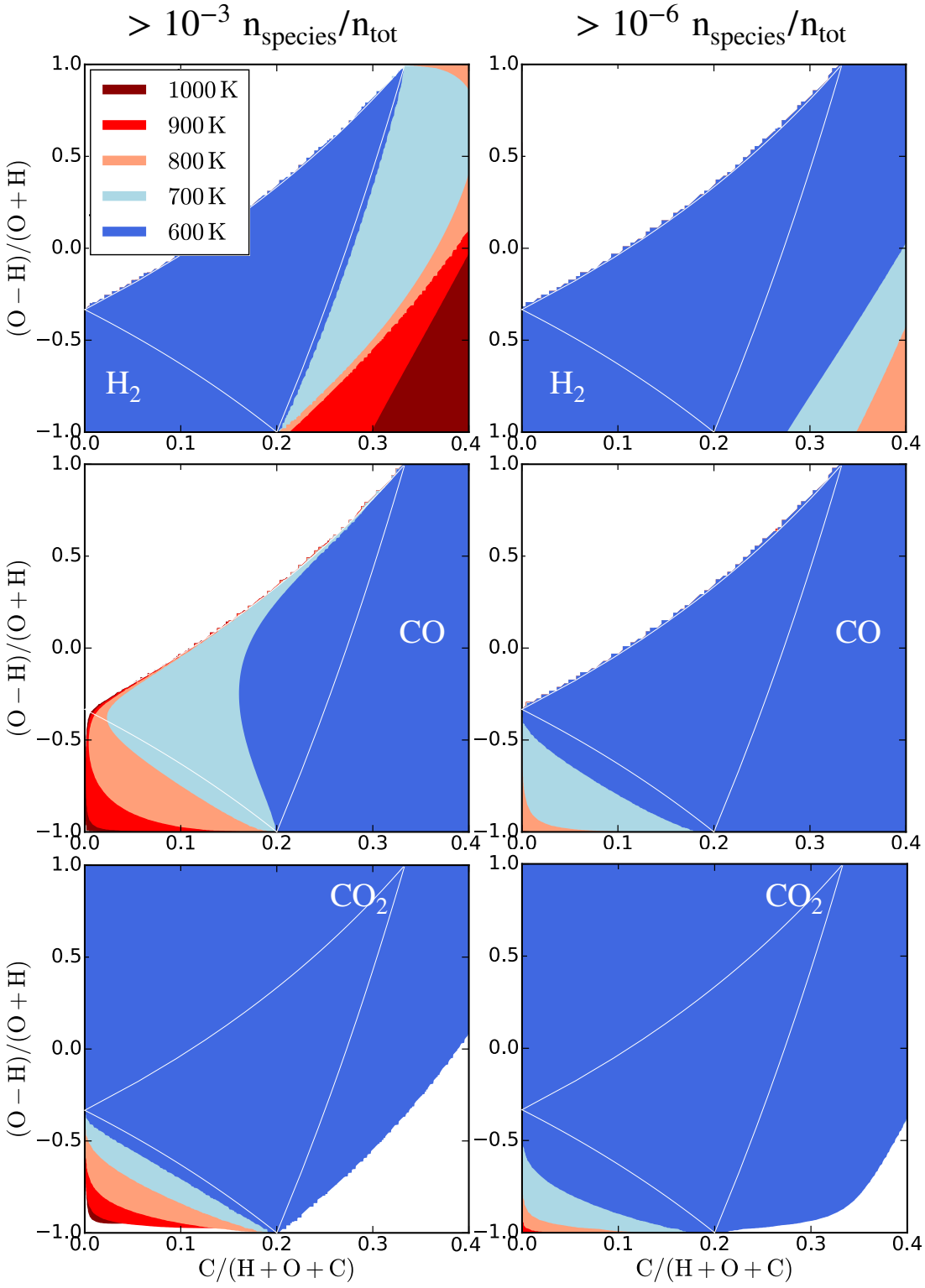

Figure 3.1: Abundances of CO_2, CO, and H_2 abundances in atmospheres at 600 K, 700 K, 800 K, 900 K, and 1000 K. Top row panels indicate areas in excess of trace abundance, the lower row panels in excess of abundant trace abundance.

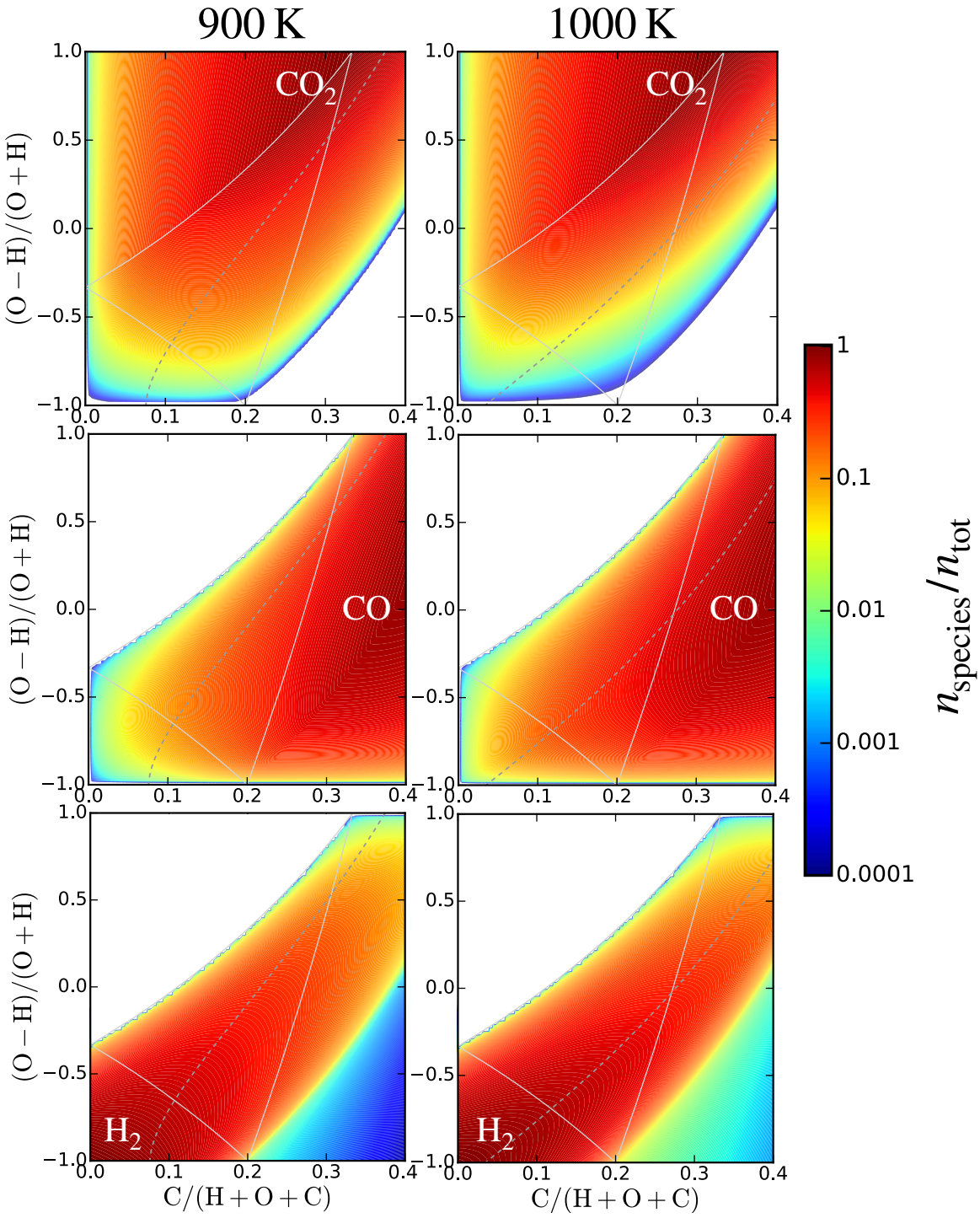

Figure 3.2: Abundances of CO_2, CO, and H_2 in atmospheres at 900 K and 1000 K. White lines indicate types following Woitke et al. (2021). The dark gray dashed line indicates where the supersaturation ration of graphite is unity. In the area to the right of this line graphite is supersaturated.

Table 3.1: Atmospheric types and molecular species coexisting in thermo-chemical equilibrium for $T > 600$ K.

Type α:	CO_2, H_2O, CH_4, CO, H_2, N_2
Type B:	H_2O, CO_2, O_2, N_2

abundance in type C, and by 700 K in excess of trace abundance in a large part of type D. By 700 K, CO is an abundant trace ($> 10^{-6}\ n_i/n_{tot}$) species in type A atmospheres and in excess of trace abundance in type C atmospheres. CO_2 is an abundant trace species in most of type A atmospheres at 700 K. At temperatures beyond 700 K all previous described trends continue, with H_2 becoming a major species across types A, C, and D, CO and CO_2 also becoming a main species in excess of trace abundance across types A, C, and D. Figure 3.2 shows abundances of CO_2, CO, and H_2 at 900 K and 1000 K. Types A,C, and D have all three molecular species above trace abundance. The three atmospheric types have become indistinguishable with increasing temperature.

Type B atmospheres are the only ones to contain significant amounts of O_2 and only contain H_2, CO, and CH_4 below trace abundances ($< 10^{-9}\ n_i/n_{tot}$). This does not change for temperatures beyond 600 K and stays consistent with the defenition by Woitke et al. (2021), up to $T = 1000$ K.

It is therefore necessary to introduce an alteration of the atmospheric type system for temperatures beyond 600 K. In the following, for temperatures $T > 600$ K, the atmospheric types will be referred to as types α and B, with type α atmospheres consisting of H_2, CO_2, H_2O, CO, CH_4, and N_2, and type B atmospheres are the same as type B for lower temperatures, with O_2, CO_2, H_2O, and N_2 as the dominating atmospheric species. In the atmospheric parameter space, type α covers the same area as the types A, C, and D would at cooler temperatures.

3.1.2 CHNOS-evolution

For most atmospheres examined in this work the bulk of the atmosphere consists mostly of the CHNO elements. However, since the elemental input abundance also include 15 further elements, in order to model the crust, sulphur was also included. In some cases sulphur is abundant enough in the input to become abundant in the models gas phase. The atmospheres resulting from the elemental input abundances of Ryugu and CI are rich in sulphur, and require a classification using the CHNOS-system under certain circumstances.

As described in Janssen et al. (2023), if the atmospheric type system from Woitke et al. (2021) is expanded by the inclusion of sulphur, new atmospheric subtypes emerge. Due to high abundances of iron in the CI and Ryugu input abundances, oxygen is depleted from the atmosphere to form various iron oxides in the crust, allowing a higher sulphur content in the atmosphere. This then allows for atmospheric models to reach these atmospheric subtypes even though sulphur abundance is a constant in the input. Following the classification scheme by Janssen et al. (2023) atmospheres modelled from the elemental inputs Ryugu and CI do reach the atmospheric subtype BC2 where SO_2 is in thermo-chemical equilibrium, coexisting with CO_2, H_2O, and N_2 and exceeds trace abundance ($> 10^{-3}\ n_{SO_2}/n_{tot}$).

Between types B and C/α, atmospheric compositions transition from an oxidising to more

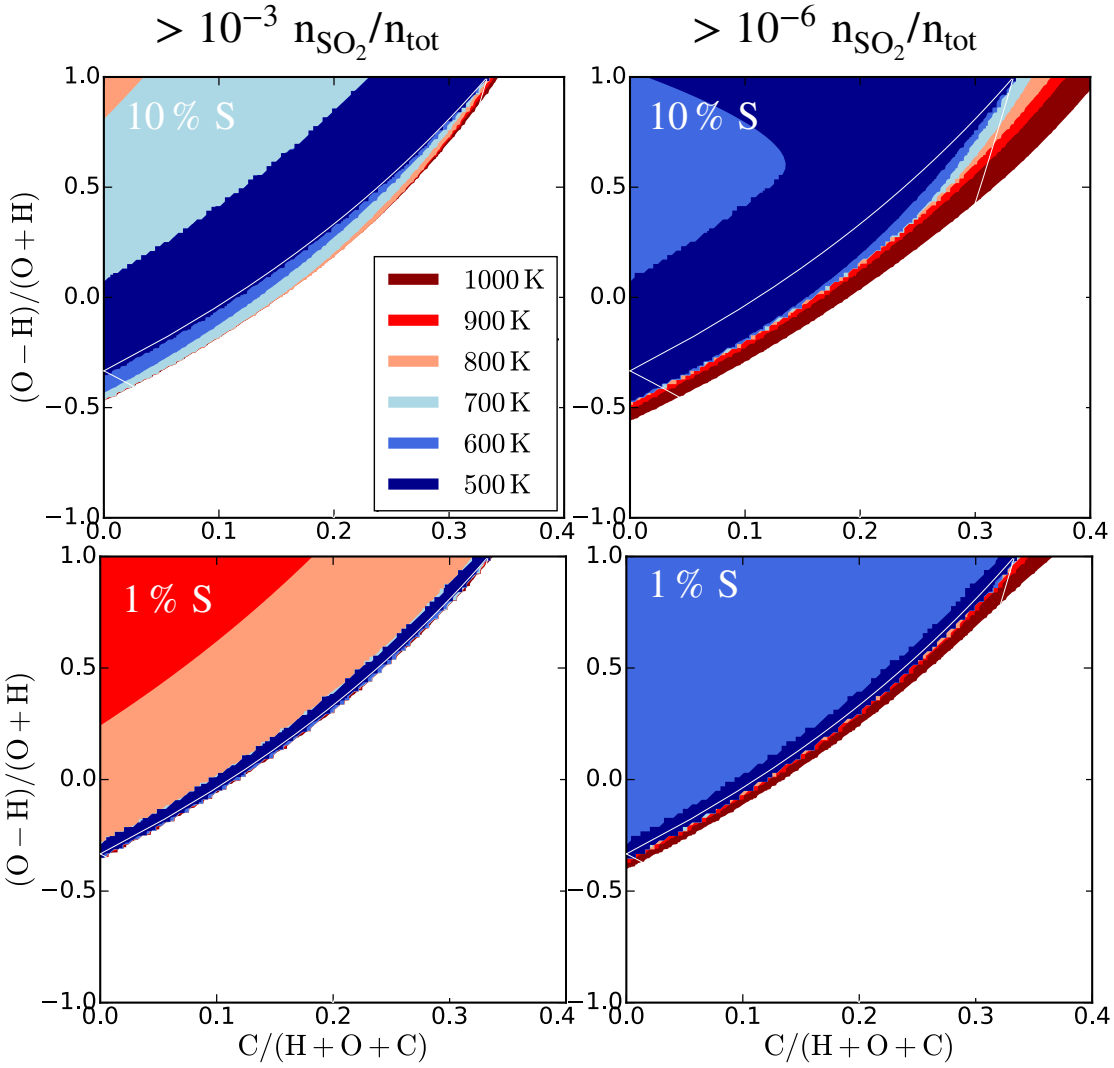

Figure 3.3: Atmospheric SO_2 abundace over temperature. The upper panels with 10 % sulphur input, the lower with 1 % sulphur input. With one percent sulphur input, SO_2 above trace abundance (and therefore the subtype BC2) stays constrained to a thin band up to 700 K. With 10 % sulphur input, type BC2 already occupies a large region in the parameter space at 500 K.

reducing compositions. This transition happens suddenly in a thin band along the atmospheric type border. Nonetheless, in this thin region a gradual change in atmospheric composition with slightly different properties from both bordering atmospheric types can be observed.

The the bulk of the atmospheres in this transitional band is made up of H_2O, CO_2, and N_2. Reducing species, such as H_2, only occur in trace or abundant trace amounts. CH_4 only occurs in trace amounts in atmospheres closer to type C/α. Sulphur containing species occur in trace to abundant trace amounts, and form a sequence in redox potential. Atmospheres closer in composition to type C/α, contain H_2S in abundant trace amounts, and more oxidising species such as SO_2, COS, and S_2 only in trace amounts. In atmospheres closer to type B atmospheric compositions, this trend reverses, and they contain abundant trace amounts of SO_2, COS, and S_2, and less H_2S compared to the more reducing atmospheres closer to type C/α. These kinds of atmospheres form a sequence from reducing to oxidising compositions and do form a distinct but not homogenous atmospheric subtype. In the following this transitional type atmospheres will be referred to as type T atmospheres.

In the elemental inputs sulphur ranges from a constant 0.027 to 5.7 percent mass fraction, depending on the used input abundance list (see Table 2.2). However, complex chemical interactions with refractory elements can allow for varying amounts of sulphur in the atmosphere, ranging from below trace abundance up to 40% number density of the atmosphere made up by sulphur species. Hence it is important to be able to gauge how much sulphur needs to present in the atmosphere until the previously described atmospheric subtypes become relevant. Small atmospheric abundances (1% number density atmospheric sulphur) and lower temperatures (500 K, 600 K) lead to very narrow atmospheric subtypes, which are most relevant for atmospheric compositions close to type T. High temperatures ($T > 700$ K) and/or high sulphur abundances (>1% number density atmospheric sulphur), lead to large regions of stability of sulphur compounds in a CHO atmospheric parameter space. This is shown in Fig. 3.3. In type BC2 atmospheres, SO_2 replaces O_2 (see also type BC1, BC2, BC3 in Janssen et al. (2023).

3.2 Crust-atmosphere link

A total of 34, 34, 48, 53, 48, and 61 unique condensates across the model grids with temperatures of 1000 K, 900 K, 800 K, 700 K, 600 K, and 500 K, respectively have been recorded. Throughout all crust-atmosphere models only a handful of condensates appear in every grid based on the different elemental input compositions. These vary with surface temperature. Some appear in crusts contacting atmospheres across the entire parameter space. Only a few condensates have limited regions of stability throughout the atmospheric parameter space, making them indicators of a crust-atmosphere link. These twelve condensates are listed in Table 3.2.

The second largest group by number are sulphur containing compounds with three condensates. These compounds show a stable link to the atmospheric type across all temperatures, with only minor evolution. This could be because sulphur can act both as refractory and volatile. Sulphur compounds and the interaction with atmospheric sulphur-rich subtypes are described in Sect. 3.2.1.

Most numerous are iron containing condensates, with six condensates (FeS and FeS_2 are also in the sulphur group), which are closely linked to the atmospheres redox potential. The combined

Table 3.2: Crust condensates exhibiting link across different surface temperatures.

	500 K	600 K	700 K	800 K	900 K	1000 K
$CaSO_4$[s]	T, BC2, B	T, BC2, B	T, BC2, B	T, BC2, B	BC2, B	B
Fe_2O_3[s]	T, BC2, B	T, BC2, B	BC2, B	B	B	B
Mn_2O_3[s]		B	B	B	B	B
TiO_2[s]	B					
MgF_2[s]	(A), T, B					
Al_2O_3[s]∗	BC2	BC2	(BC2)	(B)	(B)	(B)
FeS_2[s]	T, BC2	T, BC2	T,BC2	T,BC2		
Fe_3O_4[s]	C, (A)	(C), T	T	T, BC2	T, BC2	T, BC2
$Mn_3Al_2Si_3O_{12}$[s]	(A), (C), T	A, C, T, BC2	α,T,BC2	α, T, BC2	α, T, BC2	α, T, BC2
FeS[s]	A, C, T	A ,C, T	α,T	α, T	α, T, BC2	α, T, BC2
$FeTiO_3$[s]	(A), (C)	A, C	α	α	α	α
Fe_2SiO_4[s]	A	A, (C)	α	α	α	α

Notes: Existence of a crust species at a certain temperature is indicated with which atmospheric type(s) the condensate exists. If the type is in parentheses the condensate only exists there depending on input composition.
∗: Al_2O_3[s] is not present in all model grids, but this is due to it existing exclusively in crusts contacting type BC2 atmospheres, which were only reached by CI and Ryugu based model grids.

average oxidation state of the compounds is linked to the atmosphere. More than the six linked compounds are present, and contribute to the crusts iron oxidation state. Notably, pure iron (Fe[s]), is not directly linked to atmospheric type but is constrained to a small region in parameter space. The crusts containing pure Fe[s] are in contact with strongly reducing atmospheres, with high hydrogen and carbon abundances. Iron oxidation state and iron compounds are described in Sect. 3.2.2.

Two manganese species appear to be linked to atmospheric type. These are described in Sect. 3.2.3.

Further condensate species also link to the corresponding atmospheric types, discussed in Sect. 3.2.4.

Pure graphite (C[s]) is also not directly linked with atmospheric type, but also has a limited range of stability. It is only found in crusts in contact with atmospheres with the highest possible carbon content, where $S_{Graphite} = 1$.

3.2.1 Sulphur Chemistry

3.2.1.1 Crust Condensates

There are three species of sulphur compounds which exhibit clear links to atmospheric type, namely calcium sulfate ($CaSO_4$[s]), iron disulfide (FeS_2[s]), and iron sulfide (FeS[s]).

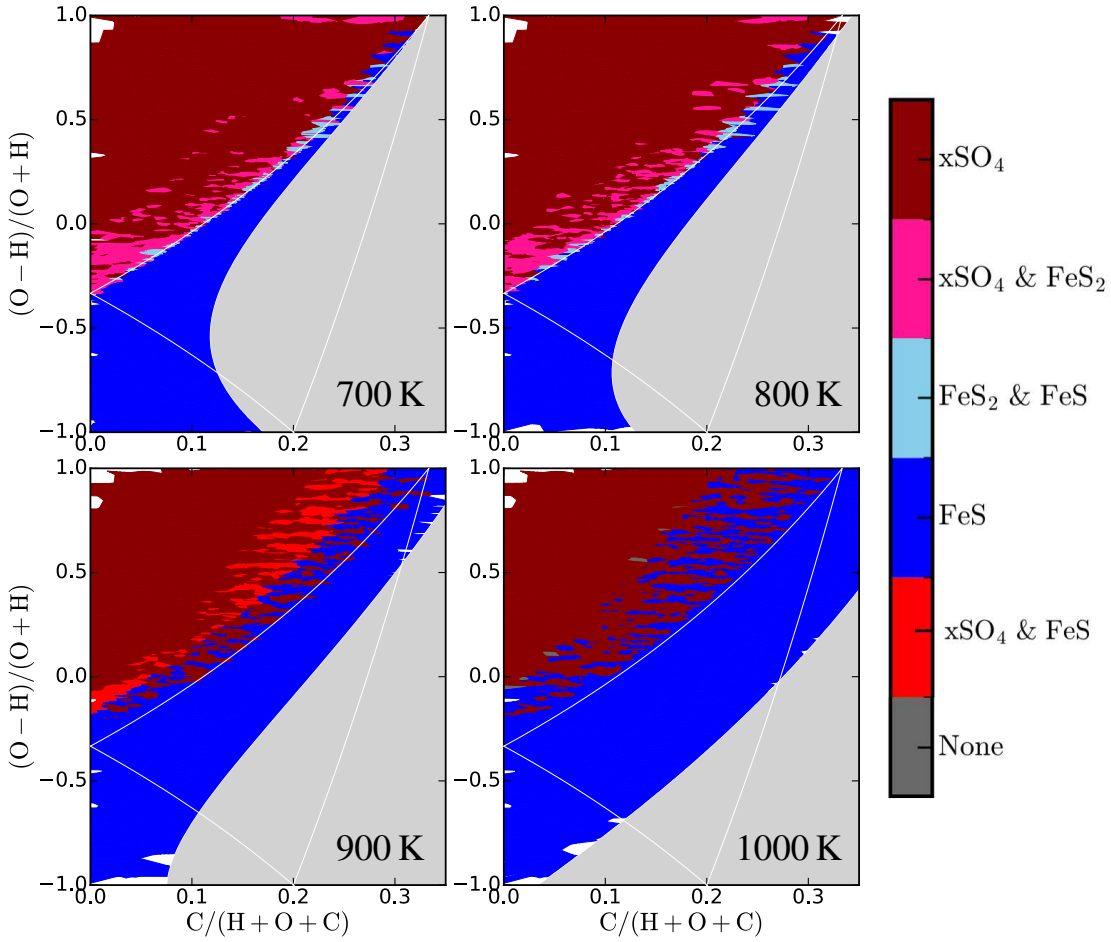

Figure 3.4: Temperature evolution of subtype BC2 and transitional regime between B and C, illustrated using the Ryugu based set of elemental input abundance. Thermal stability of FeS_2[s] ends at 900 K and it is replaced by FeS[s]. Crusts without sulphur exist when in contact with sulphur rich type BC2 atmospheres at 1000 K.

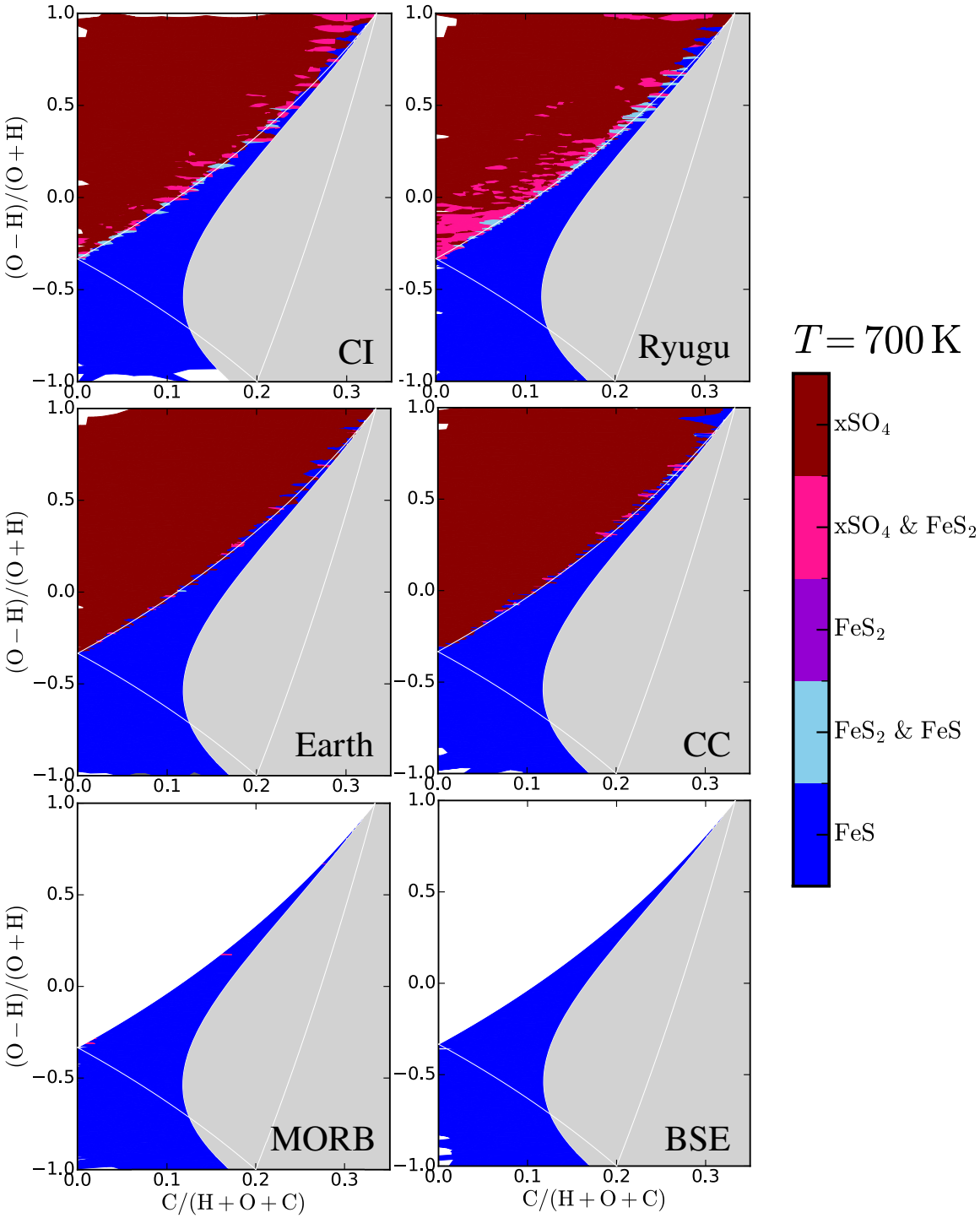

Figure 3.5: Solid sulphur in crusts at 700 K for all used input abundances (indicated in each plot). Transition from $\mathrm{xSO_4}$[s] (x: Ca, $\mathrm{K_2}$, Fe) in crusts contacting type B atmospheres, to FeS[s] in crusts contacting type α atmospheres. CI and Ryugu based grids have the atmospheric subtype BC2, which can overlay with parts of type B in a CHO parameter space. Note that BSE and MORB elemental inputs do not allow for the generation of oxygen dominated type B atmospheres. Regions where the supersaturation ratio of carbon would exceed 1 are greyed out.

$CaSO_4$[s] is found in crusts contacting type B, type T, and type BC2 atmospheres. $CaSO_4$[s] is the dominating sulphur containing species in crust-atmosphere pairs with type B atmospheres, where it is found in every model crust (brown colour in Fig. 3.5) and across all the examined temperatures. Furthermore, $CaSO_4$[s] is found in combination with either FeS_2[s] or FeS[s] depending on temperature, in type BC2, where the atmospheric composition consists of a significant amount of SO_2 (pink colour in Fig. 3.5). At high temperatures and high sulphur abundances, $CaSO_4$[s] stops appearing in crusts contacting type BC2 atmospheres, this is displayed in Fig. 3.4. Also in BC2 subtypes, in some instances, $CaSO_4$[s] is replaced or appears in combination with Iron(II) sulfate ($FeSO_4$[s]) or Potassium sulfate (K_2SO_4[s]). This does depend on the given set of total element abundances. These two condensate species only occur in the grids based on CI and Ryugu abundances, which have Fe/Ca ratios of 20.05 and 14.35 respectively, compared to 1.12 for the Earth and CC elemental input abundances. On the contrary, the K/Ca ratios in the CI and Ryugu based elemental input abundances are lower than the model grids where K_2SO_4[s] does not appear, with K/Ca ratios of 0.058 and 0.038 for the CI and Ryugu based elemental input abundances, compared to K/Ca ratios of 0.55 in both Earth and CC based models. The existence of K_2SO_4[s] can be explained with the higher sulphur availability in CI and Ryugu based elemental inputs (see Tab. 2.1). Its appearance in crusts contacting type T atmospheres is described in the following section, Sect. 3.2.1.2.

FeS_2[s] is found in crusts contacting atmospheres in the narrow transitional atmospheric type T and in sulphur rich subtype BC2. Type T atmosphere's crusts often contain a combination of either FeS_2[s] with $CaSO_4$[s], or FeS_2[s] with FeS[s]. It is also possible for FeS_2[s] to be the only stable sulphur condensate. Crusts in contact with the sulphur rich subtype BC2 atmospheres contain FeS_2[s] together with $CaSO_4$[s]. Due to the thermal stability of FeS_2[s], it stops appearing in crust-atmosphere pairs with $T > 800\,\mathrm{K}$ (Jovanović 1989). Beyond this temperature it is replaced by FeS[s] in type BC2 atmosphere's crusts. This replacement is shown in Fig. 3.4. The influence of type T atmospheres on crust FeS_2[s] existence is described in Sect. 3.2.1.2.

FeS[s] is found in crusts contacting atmospheres of type A, C, and α, where it is the only sulphur containing compound, with one exception, namely, reducing atmospheres at the very bottom of the atmospheric parameter space. It is also found in crusts contacting type T and BC2 atmospheres. Under most reducing conditions, the compounds MnS[s], MgS[s], and CaS[s] are the predominant crust sulphur species. This is caused by the availability of iron, which under such reducing conditions is predominantly found in its pure form Fe[s], instead of FeS[s]. In type BC2 atmosphere's crusts, from $T \geq 900\,\mathrm{K}$ onwards, FeS[s] first replaces FeS_2[s] and co-exists with $CaSO_4$[s], until at $T = 1000\,\mathrm{K}$ FeS[s] becomes the only sulphur species in these crusts. In summary, in crusts contacting type A and C atmospheres at 500 K and 600 K, and in crusts contacting type α atmospheres, FeS[s] is the only sulphur compound present (with the previously described exceptions).

To summarise, crusts in contact with the most reducing atmospheres contain sulphur in the form of MnS[s], MgS[s], or CaS[s]. Less reducing type A atmosphere's crusts, and all of type C and α atmospheres crust contain sulphur as FeS[s]. In the transition regime, crusts contacting type T atmospheres contain a mixture of FeS[s], FeS_2[s], and/or $CaSO_4$[s]. Crusts contacting type B atmospheres contain predominantly $CaSO_4$[s]. Type BC2 atmosphere's crusts contain $CaSO_4$[s] combined with FeS_2[s], with some outliers containing $FeSO_4$[s] or K_2SO_4[s] instead of

$CaSO_4$[s]. This is shown in Fig. 3.5. For the hotter models ($T \geq 800$ K), with input element sets based on Earth and CC, crusts in contact with atmospheres of type T can be void of any sulphur. For the model grids that also reach the sulphur rich subtype BC2, crusts void of sulphur are only observed for $T = 1000$ K, and only at the oxygen-rich edge of the BC2 subtype. In those cases, all of the available sulphur is found entirely in the gas phase. The behaviour of crusts contacting type BC2 atmospheres is more closely described in the following, Sect. 3.2.1.2.

3.2.1.2 Atmospheric Sulphur: Subtypes links to crust composition

As described in Sect. 3.1.2, if the atmospheric type system based on the CHNO system from Woitke et al. (2021) is expanded by the inclusion of sulphur, new atmospheric subtypes emerge (see Janssen et al. 2023). The composition of crusts in contact with these sulphur rich atmospheres then differs from those that are not in the subtype, but have almost identical relative ratios of C, H, and O to each other, and therefore the same location in the CHO atmospheric parameter space.

For the CI and Ryugu based grids, which contain the highest Fe and S abundances in the elemental input, the sulphur atmospheric subtypes are most pronounced. The size of the subtype region is constrained by sulphur abundance in the gas phase. Following Janssen et al. (2023), the subtype found in CI and Ryugu based grids across all temperatures investigated in this work is type BC2, with SO_2 in thermo-chemical equilibrated coexistence with CO_2, H_2O, and N_2 in excess of trace abundance. Notably, at 500 K the atmospheric models with traits similar to those of the subtype BC2 models contain SO_2 as the most prevalent gaseous sulphur species. However SO_2 is only found in trace abundances compared to the major atmospheric species CO_2, H_2O, and N_2.

Crusts in contact with atmospheres in the subtype BC2 often contain compounds otherwise found in type A, C, and α mixed with compounds found in crusts contacting type B atmospheres. This is in contrast to the atmospheres C, H, and O abundances as they are often identical to type B atmospheres. From $T = 500$ K until $T = 800$ K, crusts contacting type BC2 atmospheres contain sulphur in the form of xSO_4[s] (x: Ca, K_2, Fe) in combination with FeS_2[s]. Beyond that temperature, at $T = 900$ K the crusts contacting the atmospheres with the highest SO_2 abundance contain a mixture of xSO_4[s] (x: Ca, K_2, Fe) and FeS[s], while crusts contacting atmosphere with lower SO_2 abundances contain only FeS[s]. At $T = 1000$ K all crusts contacting type BC2 atmospheres only contain FeS[s], with some extreme cases where all input sulphur is in the atmosphere, leaving the crust without sulphur (see also Fig. 3.4)

Type T atmospheres consist of H_2O, CO_2, and N_2, which are usually considered traits of type B atmospheres. However, crusts contacting these atmospheres differ from crusts in contact with type B, C, or α atmospheres. The reason for this difference is found in the trace species in the gas phase, which differ from those found in type B, C, or α atmospheres. These 'transitional' atmospheres contain the sulphur species H_2S and SO_2 in abundant trace amounts ($>10^{-6}$ n_i/n_{tot}). Furthermore, the species COS, S_2O, S_2, S_3, S_4, and SO are found in trace amounts ($>10^{-9}$ n_i/n_{tot}). These type T atmospheres are not BC2 subtype members, because of insufficient sulphur content, but still show similar behaviour for contacting crusts compositions.

There are three main forms in which sulphur is found in the crust contacting the transitional atmospheric regime when below 900 K. First is FeS[s] with FeS_2[s] (light blue in Figs. 3.4 and 3.5). The most abundant trace atmospheric sulphur species found in atmospheres contacting

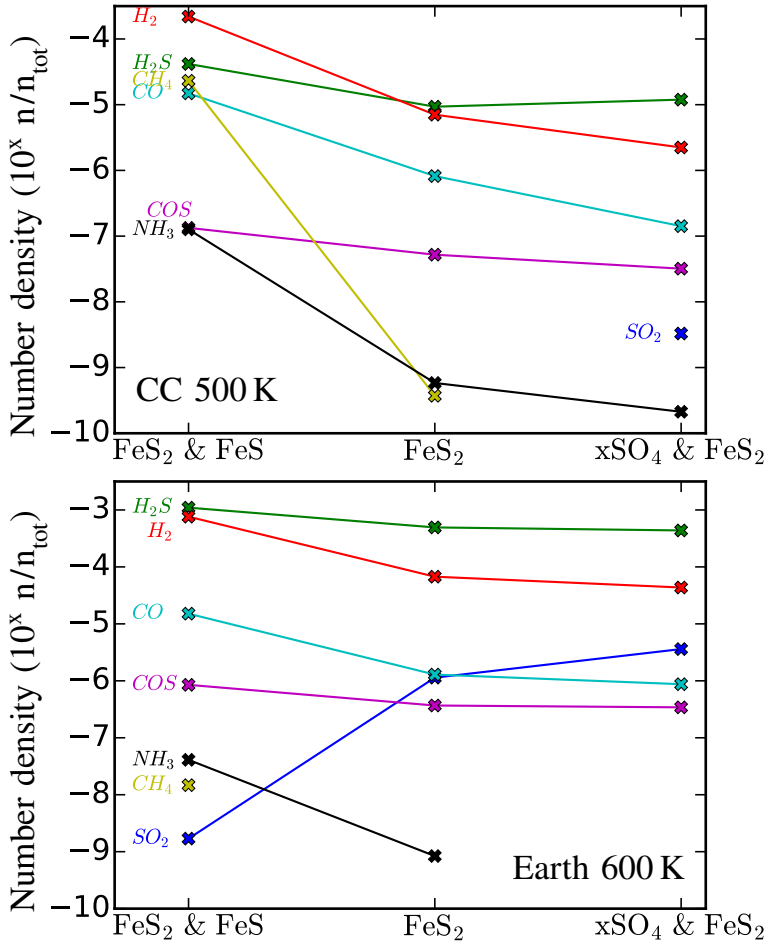

Figure 3.6: Type T atmospheric trace species. Three distinct crust sulphur compound combinations on the horizontal axis. The atmospheric composition is averaged over all type T atmospheres of the respective distinct crust compositions. A decreasing trend in reducing species, with a simultaneous rise of SO_2 is apparent.

these crusts is H_2S (except at 800 K where SO_2 becomes the dominant trace sulphur species). The general atmospheric composition under which crust-sulphur exists in the form of FeS[s] combined with FeS_2[s] is slightly reducing, with species like H_2 and HCl occurring in abundant trace amounts (see Fig. 3.1). The second way sulphur can exist in crusts touching a transitional type atmosphere is pure FeS_2[s] (purple in Fig. 3.5). The atmospheric composition is similar to the FeS[s] with FeS_2[s] containing crusts atmosphere, but reducing species become less abundant and oxidising species such as SO_2 become more abundant. The third variation of solid sulphur in contact with transitional atmospheres is xSO_4[s] with FeS_2[s] (x: Ca, K_2, Fe; pink in Figs. 3.4 and 3.5). These are the most oxidising atmospheric compositions of the three transitional atmospheres. The atmospheric sulphur species SO_2 is higher than in the previously describe transitional atmospheric types, with reducing species abundances further diminished. This is displayed in Fig. 3.6. Since the transition from FeS[s] with FeS_2[s], to FeS_2[s], to xSO_4[s] with FeS_2[s] occurs very suddenly, the gradient from reducing to oxidising environment is not clearly visibly in the interpolated atmospheric parameter space (see e.g. Fig. 3.5) but is visible when plotting abundances as in Fig. 3.1.

For temperatures beyond 800 K FeS_2[s] loses thermal stability and is replaced with FeS. In the model grids based on Earth and CC, at temperatures above 800 K, no sulphur is found in crusts in contact with transitional atmospheres. This can be explained by the low input abundance of sulphur, which is only thermally stable in the gas phase atmospheric species.

3.2.2 Iron chemistry

Iron chemistry in the crust is largely governed by how reducing or oxidising the atmosphere is. Fourteen iron containing condensates have been recorded in the models, six of which exhibit links to the atmospheric type. The remaining eight condensates are specific to the elemental input abundance, but are nonetheless constrained by how reducing or oxidising the atmosphere is. Solid iron condensates can be grouped into how oxidised the iron component is, leading to groups of

Fe(0): Fe[s];

Fe(II): FeO[s], FeS[s]*, FeS_2[s]*, Fe_2SiO_4[s]*, $FeTiO_3$[s]*, $FeAl_2O_4$[s], $Fe_3Si_4O_{12}H_2$[s], $FeAl_2SiO_7H_2$[s], $FeSO_4$[s];

Fe(II)(III): Fe_3O_4[s]*;

Fe(III): Fe_2O_3[s]*, $NaFeSi_2O_6$[s], $Ca_2FeAl_2Si_3O_{13}H$[s].

Condensates marked with * are linked to atmospheric types as described in Tab. 3.2, and Sect 3.2.2.1.

Iron compounds with less oxidised iron like Fe(II)-compounds are generally found in crusts contacting the atmospheric types A, C, α, BC2, and T. Fe_2SiO_4[s] is found in crusts contacting type A and α atmospheres. $FeTiO_3$[s] is found in crusts in contact with type A, C, and α. FeS[s] is found in crusts touching type A, C, α, T, and BC2. FeS[s] only starts appearing in crusts contacting type BC2 atmospheres beyond 800 K. FeS_2[s] exists in crusts contacting atmosphers of type T and BC2, until it loses thermal stability beyond 800 K.

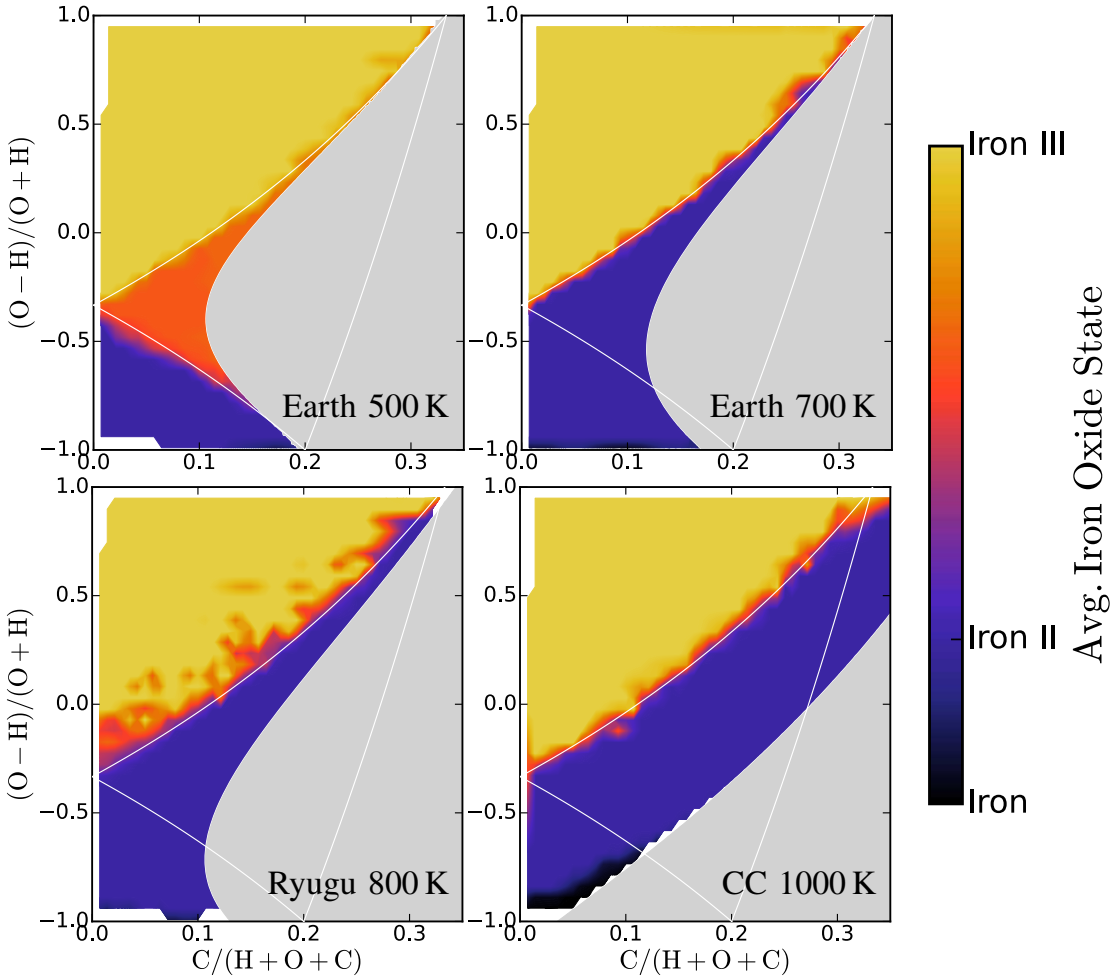

Figure 3.7: The left upper panel displays a low temperature case with distinct type A and C crust compositions. The right side upper plot shows the nominal case with a transition from Fe(0) to Fe(II) and to Fe(III) crusts, including the thin type T transition region. The left hand side lower plot includes behaviour of crusts in contact with sulphur rich subtype BC2 atmospheres, where despite similar H, C, and O abundances to type B the Iron state is between Fe(II) and Fe(III). The lower right panel shows a high temperature case without sulphur rich subtype. Pure iron can be found under the most reducing conditions.

The only Fe(II)(III) compound, Fe_3O_4[s] appears in crusts contacting type C atmospheres at 500 K, type T atmospheres from 600 K to 1000 K, and type BC2 atmospheres from 800 K to 1000 K.

The only linked Fe(III) compound, Fe_2O_3[s] is naturally found in the more oxidising atmospheric types T, BC2, and B. It appears in crusts touching type T at 500 K and 600 K. In crusts contacting type BC2 atmospheres, it is found at temperatures ranging from 500 K to 700 K. It is also found in crusts contacting type B atmospheres across all examined temperatures.

Throughout all temperatures examined in this work only the most reducing environments (H_2 and CH_4 rich atmospheres, small section of type A/α) allow for pure iron to exist in the crust, leading to crusts with the average iron oxidation state of close to Fe(0). However, the majority of crusts in contact with atmospheres of the types A or α have an average iron oxidation state close to Fe(II) or slightly above.

At 500 K and 600 K the average iron oxidation state of the crust contacting type C atmospheres can either be the same as crusts contacting type A atmospheres (close to Fe(II)) or differ slightly (close to 2.5 or above), depending on the elemental input abundance. At temperatures above 600 K, crusts in contact with type A and C atmospheres both have the iron oxidation state of around Fe(II). At higher temperatures, $T > 600$ K, when type α atmospheres come into existence, crusts contacting this type have the average iron oxidation state of around Fe(II). Type T and type BC2 atmospheres (described in Sect. 3.1.2 and Sect. 3.2.1.2) are generally more oxidising environments, which is also reflected in the contacting crusts average iron oxidation states. The corresponding crusts iron oxidation states lie firmly between Fe(II) and Fe(III), at an average of 2.5 or slightly above. Type B atmospheres are, per definition, the most oxidising environment, which is why the only existing iron state in crusts contacting type B atmospheres is Fe(III). All described cases are displayed in Figure 3.7.

3.2.2.1 Linked iron species

As previously mentioned, the atmospheres oxidising or reducing properties heavily influence the oxidation state of solid iron in the crust. Iron can occur in Fe(0), Fe(II), Fe(II)(III), and Fe(III) oxidation states, which are each found in specific condensates. Therefore, the atmospheric type cannot only be linked to the oxidation state of solid iron in the crust, but also to certain iron species.

For iron to exist in its unoxidised pure form Fe[s], strong reducing conditions are needed. These conditions are found in type A atmospheres which are rich in H_2 and CH_4, which can be seen in Fig. 3.7 in the upper and lower right hand side panels. A slender region in the bottom right of type A atmospheres provides the conditions needed for pure iron to form.

The next higher oxidation state of iron is Fe(II) which requires moderately reducing conditions found in type A, C, α, BC2, and T atmospheres. Species found in crusts contacting these types are iron(II) sulfide (FeS[s]), fayalite (Fe_2SiO_4[s]), and pyrite (FeS_2[s]). FeS[s] is found in crusts contacting type A and C up to 600 K, contacting type α atmospheres up to 1000 K, and contacting type BC2 atmospheres across all temperatures. Fe_2SiO_4[s] is constrained to type A contacting crusts for lower temperatures (500 K, 600 K), but is found in all crusts contacting type α atmospheres at 700 K to 1000 K. Despite being an iron(II) compound, FeS_2[s] is found under the more oxidising conditions of type BC2 atmospheres and type T atmospheres.

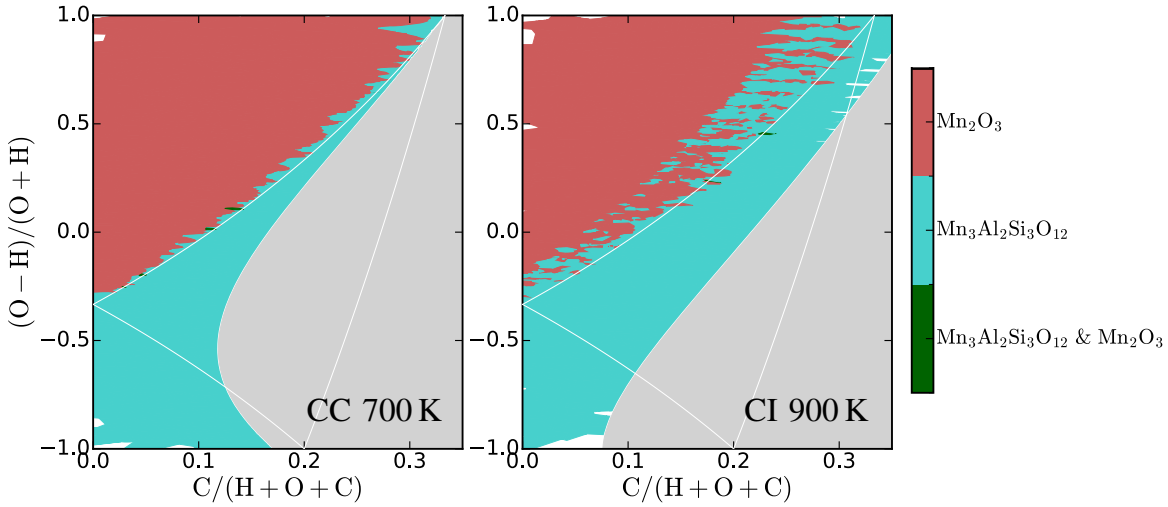

Figure 3.8: $Mn_3Al_2Si_3O_{12}$[s] and Mn_2O_3[s] in the atmospheric parameter space. The left panel displays a model grid without atmospheric type BC2, the right panel with.

Fe(II)(III) compounds need less reducing but not too strongly oxidising conditions, which are found in type C, type T atmospheres, and in type BC2 atmospheres. Iron(II)(III) oxide (Fe_3O_4[s]) is the only iron(II)(III) compound observed in models generated in this work. At 500 K it appears in crusts contacting type C atmospheres. Depending on elemental input abundance, Fe_3O_4[s] can also appear in crusts contacting less reducing parts of type A (using the CI elemental input abundance). At 600 K it appears in crusts contacting type T atmospheres and in crusts contacting type BC2 atmospheres. Additionally, it is also found in type C atmospheres, when using the CI and Ryugu elemental input abundances. At 700 K and beyond it is only found in crusts contacting type BC2 and type T atmospheres. Its effect on the crust iron oxidation state of type C contacting crusts at low temperatures can be seen in the upper left panel of Fig. 3.7. In the lower left panel of Fig 3.7 its influence on type BC2 contacting crusts iron oxidation state is clearly visible. In both right hand side panels its presence in type T atmosphere's crusts is apparent.

The most oxidising atmospheric type is type B. Under these conditions iron occurs in the form of Fe(III) exclusively. The only Fe(III) compound linked to this type is iron(III) oxide (Fe_2O_3[s]). It occurs in all crusts contacting type B atmospheres across all examined temperatures in this work. Fe_2O_3[s] also appears in crusts contacting type T atmospheres at 500 K and 600 K, and contacting type BC2 atmospheres from 500 K to 700 K.

3.2.3 Manganese species

The manganese species spessartine ($Mn_3Al_2Si_3O_{12}$[s]) and manganese(III) oxide (Mn_2O_3[s]) are both linked to atmospheric type. At 500 K spessartine containing crusts are only found contacting type T atmospheres. However, the grids based on the elemental input abundances Earth and CC yield spessartine containing crusts for all of type A and C atmospheres contacting crusts. The existence of Mn_2O_3[s] depends on the given elemental input abundance, and it does not

exist in all model grids. At 600 K spessartine exists in crusts contacting type A, C, BC2 and transitional subtype atmospheres. Mn_2O_3[s] exists in crusts contacting type B atmospheres. In Earth- and CC-based grids it only exists in crusts contacting type B atmospheres with an (O-H)/(O+H) ratio above 0.4, for ratios below 0.4, piemontite ($Ca_2MnAl_2Si_3O_{13}H$[s]), takes its place as the predominant manganese species. For temperatures $T \geq 700$ K spessartine exists in crusts contacting type α, T, and BC2 type atmospheres, and Mn_2O_3[s] exists in all type B atmosphere contacting crusts. Crusts contacting Type T atmospheres can also contain both $Mn_3Al_2Si_3O_{12}$[s] and Mn_2O_3[s].

In Fig. 3.8 one model grid without atmospheric type BC2 (left, CC-based) and one model grid with atmospheric type BC2 (right, CI-based) are displayed. Also visible are type T contacting crusts where both compounds co-exist.

3.2.4 Further condensates

Titanium dioxide TiO_2[s] exists in crusts contacting type B atmospheres at 500 K. In model grids based on Earth and CC elemental input abundances, crusts in contact with type B atmospheres with an (O-H)/(O+H) ratio above 0.3, TiO_2[s] is replaced with $CaTiSiO_5$[s].

Magnesium flouride MgF_2[s] exhibits a link to the atmosphere at 500 K. It exists in crusts contacting types T and B atmospheres. The grid based on the Ryugu elemental input abundance also yields MgF_2[s] in crusts contacting atmospheres below (O-H)/(O+H)<-0.8 in type A.

Aluminium oxide Al_2O_3[s] appears in crusts contacting the sulphur-rich subtype BC2 atmospheres. It only appears in model grids based on Ryugu and CI based elemental input abundances, because only those grids have sufficient sulphur abundances to reach the atmospheric subtype BC2. It appears in crusts at 500 K and 600 K. At 700 K, Al_2O_3[s] exists in crusts contacting type B atmospheres in CI and in Ryugu based model grids. Additionally, in models grids based on the Ryugu elemental input abundance, Al_2O_3[s] also exists in crusts contacting type BC2 atmospheres. For temperatures beyond 700 K, Al_2O_3[s] exists in crusts contacting type B in model grids based on CI and in Ryugu elemental input abundances.

4 Discussion

This thesis investigated the connection between atmospheric compositions and crust compositions across a large variety of atmospheric compositions, input compositions, and temperatures. It builds on previous work where indications for such a link has been shown (Herbort & Sereinig 2025). Previously ambiguous links between crust condensate groups and the atmosphere have been resolved more clearly. This has been achieved by finely sampling an atmospheric parameter space with atmosphere-crust model pairs.

4.1 Limits

The modelling method used throughout this work is based on calculating the thermo chemical and phase equilibrium chemistry between the atmosphere and crust. Although much can be learned from this, the approach comes with some caveats which have to be adequately understood and stated.

The modelling approach only took the crust and base layer of the atmosphere (the layer in direct contact with the crust) into account, but transit observations are only sensitive to the upper high altitude layers, where the atmosphere is optically thin, at pressures of 10^{-2} bar to 10^{-5} bar (Madhusudhan & Seager 2009). This means if atmospheres, close to the region where the crust composition transitions, lose their chemically unique composition with altitude, the crust composition transition is blurred in potential observations. In Herbort & Sereinig (2025), atmospheres-crust model pairs were examined to pressures of 10^{-7} bar and results indicate that atmospheric compositions do in fact change and can potentially converge or diverge. This happens with atmospheres that experience condensation, which is more pronounced at low temperatures (300 K, 400 K surface temperature), as H_2O can condense along the atmospheres pressure-temperature-profile ((p,T)-profile). Atmospheres can also experience graphite condensation, which can cause to surface level type C atmospheric compositions to change to type A atmospheric compositions at high altitudes where the pressure is low. This effect is less pronounced at higher temperatures (see Herbort et al. 2022; Herbort & Sereinig 2025). It is reasonable to assume that higher temperatures will lead to even less compositional change along the atmospheres (p,T)-profile. To gauge how well surface composition transitions will be observable further study is needed, potentially with a similar grid with atmospheric (p,T)-profiles down to lower pressures.

Byrne et al. (2024) demonstrate that pressure and temperature changes along a (p,T)-profile can alter crust compositions when comparing low altitude with high altitude regions on the example of Venus. In this, similarly sharp transitions (as in Sect. 3.2.1, Sect.3.2.2), Sect. 3.2.3 from one condensate to the other were described. This motivates further future investigations of changes of the crust compositions with pressure changes.

The shape of the (p,T)-profile also influences the chemistry and therefore the composition of a planets atmosphere. The shape is governed by the received stellar flux, how efficiently this flux is absorbed by atmospheric species, the planets surface reflectivity, clouds, and the planets equilibrium temperature. Simple models such as a polytropic profile (e.g Herbort et al. 2022) or profiles which become isothermal at high altitudes (see also Herbort & Sereinig 2025) can serve as good approximations. Future works might incorporate stellar flux into the (p,T)-profiles calculation (e.g. implemented in Min et al. (2020)).

Exoplanets are spherical objects. This means the modelling approach used in this thesis neglects any effects caused by the shape of real life exoplanets e.g. the fact that half of any given planet experiences night leads to temperature differences between the day and night side. In extreme cases, tidally locked planets experience eternal day or night on either side of the planet, with extreme thermal gradients. Also the influence of incoming stellar flux differs with longitude. More direct flux is received close to the planet's equator when compared to the poles, which in turn influences the temperature and composition.

Atmospheric dynamics like convective motion have not been considered in this work. Depending on the efficiency of convection, it could restore chemical composition altered by condensation (e.g. Smith 1998). This could make atmospheres which converge due to condensation distinguishable again, and make crust composition transitions more accessible for observations.

The choice of thermo chemical and phase equilibrium chemistry for the modelling does neglect important processes like such as outgassing, volcanism, atmospheric escape, and photochemistry. What composition an atmosphere and crust have is also heavily governed by the interior of the planet (e.g. Gaillard & Scaillet 2014; Schaefer et al. 2012), which is beyond the scope of this work. Linking planetary interior and the atmospheric composition is the subject of active research (e.g. Spaargaren et al. 2020). Additionally, GGchem only provides a list of stable molecules and atoms for the condensate phase. These condensates can form solid solutions, which could be modelled in the future using tools like Perplex_X (Myhill & Connolly 2021).

The overall element availability does play a big role in the final composition of a planet. In this work the use of different elemental input abundance lists were used to prevent biases. Nonetheless, all elemental input abundance lists are based on bodies of the solar system, which in itself is a bias towards the solar systems composition. To generate models with crust compositions that are as accurate and complete as possible, 18 input elements were used. Abundances of protoplanetary disks could inform exoplanet modelling, but currently focus on mostly volatiles (e.g. Keyte et al. 2024). Future observation might provide more complete elemental abundance measurements to inform exoplanet (crust and bulk composition) modelling.

4.2 Implications

The condensates described in Table 3.2 are linked to atmospheric type. That means if there is a transition among a certain group of linked condensates (e.g sulphur containing compounds, Sect. 3.2.1) the transition coincides with atmospheric type transitions. That means that for any given O/H and C/O ratios of an atmosphere any given state of the corresponding crust can exist. For a clear unambiguous description of the crust based on atmospheric composition it is necessary to take the y coordinate, defined as (O-H)/(O+H) and x coordinate, defined as C/(H+O+C), of the

atmosphere in the CHO parameter space into account. To further complicate the problem, it is also necessary to measure sulphur abundances in the atmospheres. Above 1% sulphur content, an atmosphere could potentially fall into an atmospheric subtype defined by sulphur species above trace abundance, which changes the crusts composition compared with crusts contacting atmospheres with the same x and y coordinates in the CHO parameter space.

In summary, an accurate prediction of crustal composition based on atmospheric composition measurements would require C, H, O, and S abundance measurements. Current observational capabilities are on the cusp of potentially meeting those requirements (see e.g. Hu et al. 2024), and are set to improve in the future.

With the findings of this work the highly degenerate question of constraining compositions of terrestrial exoplanet surfaces is a step closer to being answered. The findings of this work do not require new observational techniques, but utilise existing and constantly improving observational techniques such as transit spectroscopy. The transitions of surface mineralogy are stark and often stable over a range of temperatures. The link between crust and atmosphere is also heavily governed by atmospheric type, which might be of help for future observations. This means that observations do not have to be precise enough to constrain the exact CHO parameter space position of the atmosphere, but it would be enough to constrain the atmospheric type of the observed atmosphere in order to constrain the surface composition.

5 Summary

In this thesis atmospheric and crustal compositions of rocky exoplanets were modelled in a grid like fashion across an atmospheric parameter space. Six sets of total element abundances as inputs were used to create grids at each 500 K, 600 K, 700 K, 800 K, 900 K, and 1000 K. The elemental input abundances consisted of 18 elements. To create the grid of crust-atmosphere models across an atmospheric parameter space, the abundances of C, H and O were slightly varied from grid point to grid point. The remaining 15 elements were kept constant by keeping the sum of C+H+O the same between each grid point. This constraint limited the volatile CHO budget, which prevented two input abundances from forming full parameter spanning grids. The chemical modelling was done under the assumption of thermo-chemical and phase equilibrium. The pressure was assumed as constant, as only the atmospheric layer in immediate contact with the crust was modelled. This approach resulted in 24 full grids and 12 partial grids across the investigated temperatures, with each consisting of around 5000 crust-atmosphere model pairs.

The atmospheric classification system by Woitke et al. (2021) has been expanded to temperatures of 1000 K with the introduction of the new atmospheric type α. Type α atmospheres arise at 700 K when the previously distinct types start to merge into one. At this temperature the majority of atmospheric compositions in type A contain CO and CO_2 in abundant trace amounts ($> 10^{-6}\, n_i/n_{tot}$) and all type D atmospheres contain at least abundant trace amounts ($> 10^{-9}\, n_i/n_{tot}$) of H_2. In type A atmospheres, NH_3 abundances fall below trace abundance. This trend continues towards higher temperatures until the compositions of type A, C, and D atmospheres become indistinguishable and form the new atmospheric type α. The composition of atmospheres in this newly formed high temperature type consists of CO_2, H_2O, CH_4, CO, H_2, and N_2 all above trace abundances ($> 10^{-3}\, n_i/n_{tot}$). Type B is unchanged at temperatures beyond 600 K, and stays consistent with its original definition.

The existence of sulphur rich atmospheric subtypes described by Janssen et al. (2023) from 500 K to 1000 K has been described when using sulphur-rich elemental inputs. Additionally, a transitional type of atmosphere between types C and B with sulphur containing trace species was observed in models based on sulphur-poor elemental inputs. This transitional atmospheric type contains more sulphur when the temperature is high (T>800 K), in some cases depleting the crust of all sulphur if the input abundance of sulphur is low.

The link between atmospheric and crustal compositions has been examined, with certain groups like sulphur containing condensates and iron containing condensates appearing to have the strongest connection to the corresponding atmospheric composition. As atmospheric types transition throughout the atmospheric parameter space, crust condensates of species examined in this work do evolve with them.

Sulphur containing condensates, namely FeS[s], FeS_2[s], and xSO_4[s] (with x: ca, K_2, Fe), are closely linked to the atmospheres composition and type. Crusts under tendentiously reducing atmospheres (types A and C) have FeS[s] present. For slightly more oxidising atmospheric

compositions (intermediate between types B and C, and type BC2), solid sulphur starts to occur in different forms in the following sequence: FeS[s] with FeS_2[s], FeS_2[s], and xSO_4[s] with FeS_2[s]. This transition is temperature dependent as the thermal stability of FeS_2[s] prohibits its formation for $T > 800$ K. FeS_2[s] is replaced by FeS[s] with some more oxidising crusts still retaining the combination of xSO_4[s] with FeS[s]. From 900 K to 1000 K, all crusts contacting type BC2 or transitional atmospheres between types B and C contain FeS[s] or no sulphur. In cases where no sulphur is found in the crust, it is found entirely in the gas phase. This is caused by the too small input abundance of sulphur in certain elemental input abundances. Crusts contacting the most oxidising atmospheric type, type B, contain sulphur solely in the form of xSO_4[s] (with x: ca, K_2, Fe) with the overwhelming majority of crusts forming $CaSO_4$[s].

The iron oxide state of the crust and iron-containing compounds are also linked to the corresponding atmospheric type. Reducing environments favour iron compounds with lower oxidation state numbers, while oxidising atmospheric compositions lead to more oxidised iron compounds in the crusts. Notably, the same atmospheric O/H ratio can lead to very different oxidation states of the the crust, depending on the carbon and sulphur contents of the atmosphere. The crusts iron oxide state is therefore heavily linked to the atmospheric type. Crusts contacting type A atmospheres oxidation state at Fe(II). Crusts contacting type C atmospheres can be Fe(II) or Fe(II)(III) depending on the elemental input abundance at lower temperatures (500 K, 600 K). Type α atmosphere's crusts oxidation state is Fe(II). Type B atmosphere's crusts oxidation state is Fe(III). Crusts, contacting atmospheres of the sulphur rich subtype BC2 and type T, oxidation state is Fe(II)(III).

A pair of manganese containing compounds are also linked to atmospheric type, namely $Mn_3Al_2Si_3O_{12}$[s] and Mn_2O_3[s]. At lower temperatures (500 K) other manganese compounds are favoured. At temperatures of $T \geq 600$ K $Mn_3Al_2Si_3O_{12}$[s] populates crusts contacting atmospheres in the types A, C, BC2, α, and transitional atmospheres between types B and C. Mn_2O_3[s] is found in crusts contacting type B atmospheres. This split can once again be explained by the reducing or oxidising properties of the atmosphere.

TiO_2[s] occurs in crusts contacting type B atmospheres at 500 K, but depending on the given elemental input abundance TiO_2[s] does not necessarily occurs in all crusts contacting type B atmospheres, but appears in crusts contacting a smaller subset of type B atmospheres.

MgF_2[s] exists in type T and B atmosphere's crusts at 500 K. Depending on the elemental input abundance MgF_2[s] can also occur under reducing conditions in crusts contacting type A atmospheres.

Al_2O_3[s] exists in crusts in contact with type BC2 atmospheres at 500 K and 600 K. From 700 K to 1000 K Al_2O_3[s] can occur in crusts contacting type B atmospheres, depending on the elemental input abundance.

In this thesis, crust-atmosphere pairs were modelled using a thermochemical and phase equilibrium chemistry based approach. Temperatures ranging from 500 K to 1000 K in 100 K increments were examined. For that, the existing atmospheric type system had to be expanded to temperatures beyond 600 K, yielding the definition of a new atmospheric type, type α. Additionally, between the types C/α and B, another new subtype of atmospheres was classified. This type, type T, bridges the gap between the two vastly different atmospheric types. Crust compounds generally follow a similar transition across atmospheric types, with a stark and sudden

transition at the atmospheric type border between type C/α and type B. Sulphur compounds transition from FeS[s] to $CaSO_4$[s], the iron oxidation states of the crust transition from Fe(II) to Fe(II), and Manganese compounds transition from $Mn_3Al_2Si_3O_{12}$[s] to Mn_2O_3[s]. Sulphur compounds and iron oxide state differ from both states in crusts contacting type T, with the unique sulphur compound FeS_2[s] being present, and the iron oxidation state being in between Fe(II) and Fe(III). The crust-atmosphere link evolves with temperature, with most crust mineral transitions being between the temperatures of 600 K and 800 K. Despite the modelling limitations, this work identifies substantial crust-atmosphere links. Combined with future observations, the findings of this work could possibly offer constraints of exoplanet surface compositions.

Bibliography

Arevalo, Ricardo, J. & McDonough, W. F. 2010, Chemical Geology, 271, 70

Barklem, P. S. & Collet, R. 2016, Astronomy & Astrophysics, 588, A96

Batalha, N. M., Borucki, W. J., Bryson, S. T., et al. 2011, Astrophysical Journal, 729, 27

Benz, W., Broeg, C., Fortier, A., et al. 2021, Experimental Astronomy, 51, 109

Berta, Z. K., Charbonneau, D., Désert, J.-M., et al. 2012, The Astrophysical Journal, 747, 35

Byrne, X., Shorttle, O., Jordan, S., & Rimmer, P. B. 2024, Monthly Notices of the Royal Astronomical Society, 527, 10748

Charbonneau, D., Brown, T. M., Latham, D. W., & Mayor, M. 2000, Astrophysical Journall, 529, L45

Charbonneau, D., Brown, T. M., Noyes, R. W., & Gilliland, R. L. 2002, Astrophysical Journal, 568, 377

Ducrot, E., Lagage, P.-O., Min, M., et al. 2025, Nature Astronomy, 9, 358

Gaillard, F. & Scaillet, B. 2014, Earth and Planetary Science Letters, 403, 307

Gardner, J. P., Mather, J. C., Abbott, R., et al. 2023, Publications of the Astronomical Society of the Pacific, 135, 068001

Gilmore, M., Treiman, A., Helbert, J., & Smrekar, S. 2017, Space Science Reviews, 212, 1511

Gilmozzi, R. & Spyromilio, J. 2007, The Messenger, 127, 3

Helbert, J., Müller, N., Kostama, P., et al. 2008, Geophysical Research Letters, 35

Henry, G. W., Marcy, G. W., Butler, R. P., & Vogt, S. S. 2000, Astrophysical Journall, 529, L41

Herbort, O. & Sereinig, L. 2025, A&A, 699, A67

Herbort, O., Woitke, P., Helling, C., & Zerkle, A. 2020, Astronomy & Astrophysics, 636, A71

Herbort, O., Woitke, P., Helling, C., & Zerkle, A. L. 2022, Astronomy & Astrophysics, 658, A180

Hu, R., Bello-Arufe, A., Zhang, M., et al. 2024, Nature, 1

Janssen, L. J., Woitke, P., Herbort, O., et al. 2023, Astronomische Nachrichten, 344

Jordan, S., Rimmer, P. B., Shorttle, O., & Constantinou, T. 2021, Astrophysical Journal, 922, 44

Jovanović, D. 1989, Journal of thermal analysis, 35, 1483

Kappel, D., Arnold, G., & Haus, R. 2016, Icarus, 265, 42

Keyte, L., Kama, M., Booth, A. S., Law, C. J., & Leemker, M. 2024, MNRAS, 534, 3576

Léger, A., Rouan, D., Schneider, J., et al. 2009, Astronomy & Astrophysics, 506, 287

Lichtenberg, T. & Miguel, Y. 2025, Super-Earths and Earth-like exoplanets (Elsevier), 51–112

Liggins, P., Jordan, S., Rimmer, P. B., & Shorttle, O. 2023, Journal of Geophysical Research (Planets), 128, e2022JE007528

Lodders, K., Palme, H., & Gail, H. P. 2009, Landolt Börnstein, 4B, 712

Madden, J. H. & Kaltenegger, L. 2018, Astrobiology, 18, 1559

Madhusudhan, N. & Seager, S. 2009, The Astrophysical Journal, 707, 24

Mayor, M. & Queloz, D. 1995, Nature, 378, 355

Min, M., Ormel, C. W., Chubb, K., Helling, C., & Kawashima, Y. 2020, Astronomy & Astrophysics, 642, A28

Myhill, R. & Connolly, J. A. 2021, Contributions to Mineralogy and Petrology, 176, 86

Piaulet-Ghorayeb, C., Benneke, B., Turbet, M., et al. 2025, The Astrophysical Journal, 989, 181

Pont, F., Knutson, H., Gilliland, R. L., Moutou, C., & Charbonneau, D. 2008, Monthly Notices of the Royal Astronomical Society, 385, 109–118

Rauer, H., Aerts, C., Cabrera, J., et al. 2025, Experimental Astronomy, 59, 26

Richardson, L. J., Deming, D., Horning, K., Seager, S., & Harrington, J. 2007, Nature, 445, 892–895

Rimmer, P. B., Jordan, S., Constantinou, T., et al. 2021, The Planetary Science Journal, 2, 133

Rustamkulov, Z., Sing, D. K., Mukherjee, S., et al. 2023, Nature, 614, 659

Schaefer, L., Lodders, K., & Fegley, B. 2012, Astrophysical Journal, 755, 41

Smith, M. D. 1998, Icarus, 132, 176

Spaargaren, R. J., Ballmer, M. D., Bower, D. J., Dorn, C., & Tackley, P. J. 2020, Astronomy & Astrophysics, 643, A44

Stock, J. W. 2008, PhD thesis, Technische Universität Berlin

Surkov, Y. A., Moskalyeva, L., Shcheglov, O., et al. 1983, Journal of Geophysical Research: Solid Earth, 88, A481

Surkov, Y. A., Moskalyova, L., Kharyukova, V., et al. 1986, Journal of Geophysical Research: Solid Earth, 91, E215

Tinetti, G., Drossart, P., Eccleston, P., et al. 2018, Experimental Astronomy, 46, 135

Tsai, S.-M., Parmentier, V., Mendonça, J. M., et al. 2024, The Astrophysical Journal, 963, 41

Van Looveren, G., Boro Saikia, S., Herbort, O., et al. 2025, A&A, 694, A310

Wakeford, H. R., Sing, D. K., Deming, D., et al. 2013, Monthly Notices of the Royal Astronomical Society, 435, 3481

Woitke, P., Helling, C., Hunter, G., et al. 2018, Astronomy & Astrophysics, 614, A1

Woitke, P., Herbort, O., Helling, C., et al. 2021, Astronomy & Astrophysics, 646, A43

Wolszczan, A. & Frail, D. A. 1992, Nature, 355, 145

Wordsworth, R. & Kreidberg, L. 2022, Annual Review of Astronomy and Astrophysics, 60, 159–201

Wyttenbach, A., Ehrenreich, D., Lovis, C., Udry, S., & Pepe, F. 2015, Astronomy & Astrophysics, 577, A62

Xue, Q., Zhang, M., Coy, B. P., et al. 2025, arXiv e-prints, arXiv:2508.12516

Yang, J. & Hu, R. 2024, The Astrophysical Journal, 966, 189

Yokoyama, T., Dauphas, N., Fukai, R., et al. 2025, The Elemental Abundances of Ryugu: Assessment of Chemical Heterogeneities and the Nugget Effect